

SPONTANEOUS EDGE CURRENT IN CHIRAL
SUPERCONDUCTORS WITH HIGH CHIRALITY

SPONTANEOUS EDGE CURRENT IN CHIRAL
SUPERCONDUCTORS WITH HIGH CHIRALITY

BY

XIN WANG, M.Eng.

A Thesis

Submitted to the School of Graduate Studies

in Partial Fulfilment of the Requirements

for the Degree of

Master of Science

McMaster University

© Copyright by Xin Wang, September 2017

MASTER OF SCIENCE (2017)
(Department of Physics and Astronomy)

McMaster University
Hamilton, Ontario, Canada

TITLE: Spontaneous edge current in chiral superconductors with
high chirality

AUTHOR: Xin Wang, M.Eng.

SUPERVISOR: Dr. Catherine Kallin

NUMBER OF PAGES: viii, 59

Abstract

We study the spontaneous edge current of chiral superconductors with high chirality both in the absence and presence of Meissner screening. We compute the edge current from a self-consistent solution to a set of coupled equations: quasiclassical Eilenberger equation, superconducting gap equation, and Maxwell equation. We find that the spatial dependent chiral edge current is largely suppressed and has more nodes for higher chirality pairings. In the absence of Meissner screening, the integrated current at $T = 0$ is zero for all higher chirality pairings; while it is substantial for chiral p -wave. This conclusion is consistent with previous studies. In contrast, at finite T , the integrated current is non-zero even for higher chiral pairings. It turns out that the spatial varying order parameter is crucial to understand this finite T behavior of the edge current. When Meissner screening is included, the magnitude of the edge currents is reduced for all chiral pairings; however, the reduction is much weaker in higher chirality cases. We conclude that the Meissner effect is not that important for higher chiral pairings. We also consider the effect of the rough surface on the edge current. The edge current of even chiral pairings is inverted by the strong surface roughness; however, that of the odd chiral pairings is not. The sub-dominant order parameters, induced by the surface, are the key to understanding this current inversion.

Acknowledgements

I owe my deepest gratitude to my advisor Prof. Catherine Kallin for her numerous support and encouragement. She has always been patient to provide guidance on my research as well as my studies. Beyond this, she offers me a lot of opportunities outside McMaster. I have always been impressed by her deep physical insight and meticulous pursuit. I feel honored and privileged to be her student.

I am indebted to the other two committee members, Prof. John Berlinsky and Prof. Erik Sorensen, for their useful suggestions on my research. I would also like to thank Prof. Peter Gordon Sutherland, Prof. Bruce Gaulin and Prof. Sung-Sik Lee for their wonderful classes which influence me beyond the thesis.

It is my honor to thank Prof. Jinshan Wu, who brought me into the world of physics. He encouraged and carefully protected my interests. His support lasts till this day.

I am grateful to Dr. Wen Huang and Dr. Zhiqiang Wang for countless discussions. They have given me many suggestions and helped me in many aspects that related to my studies. I would also like to thank Laimei Nie and Soshi Mizutani for their helpful discussions during my early stage.

I feel lucky to have a group of friends and schoolmates here to share my life and interests with: Ke Meng, Xuejiao Liu, Lili Zhang, Huifang Pang, Wenjing Hua,

Haizhao Zhi, Yipeng Cai, Qianli Ma, Sean Takahashi, Anton Borissov, Ryan Plestid and so on. I would also like to thank friends in China, Peng Zhang, Qian Zhuang, Ying Zhuang, Tianxiao Qi, Yichen Zhou, Jingwen Li, Zhesi Shen, He Li and so on, for their encouragement. Besides, I would like to thank Leo's home for the happiness they have brought me.

Lastly but most importantly, I wish to thank my parents, Xiaoguo Wang and Xiuyan Ma, for their unconditional support and love.

Contents

Abstract	iii
Acknowledgements	iv
1 Introduction	1
1.1 Chiral Superconductivity	2
1.2 Spontaneous edge current	3
1.3 Plan of this thesis	5
2 Quasiclassical Formulation	6
2.1 Quasiclassical Approximation	7
2.2 Numerical Procedure	11
2.3 Uniform Order Parameter Analysis	15
3 Self-consistent Edge Current Without Screening	20
3.1 Spatial profiles of the current density	21
3.2 Temperature dependence of the integrated current	26
4 Self-consistent Edge Current With Screening	30

5	Rough Surface Effect	36
6	Conclusions	42
A	Gor'kov Equation for Matsubara Green's Functions	45
A.1	Matsubara Green's Functions	45
A.2	Gor'kov Equation	48

List of Figures

2.1	Classical trajectory of a Bogoliubov quasiparticle.	12
3.1	Spatial profiles of the unscreened chiral order parameter components	21
3.2	Spatial profiles of the unscreened chiral edge current	23
3.3	Schematic edge dispersion for higher chirality superconductors	24
3.4	Current channels (unscreened) in higher chirality superconductors . .	25
3.5	Temperature dependence of I_y for chiral p -wave superconductors . . .	27
3.6	Temperature dependence of I_y for higher chirality superconductors . .	28
4.1	Spatial profiles of the screened chiral order parameter components . .	31
4.2	Spatial profiles of the screened chiral edge current	32
4.3	Angular dependence of the screened chiral p -wave edge current	34
5.1	Effects of the weak surface roughness on the unscreened edge current	38
5.2	Effects of the strong surface roughness on the unscreened edge current	39
5.3	Effects of the strong surface roughness on the screened edge current .	40

Chapter 1

Introduction

Superconductivity is a quantum mechanical phenomenon that has attracted considerable interest from condensed matter physicists since its discovery in 1911. By the 1960s, the discovered superconductors seemed to be fully understood by the microscopic Bardeen-Schrieffer-Cooper (BCS) theory[1] together with the phenomenological Ginzburg-Landau theory[2]. However, in 1985 the discovery of high T_C superconductivity [3] opened an age of unconventional superconductivity beyond the original BCS theory and brought attention to the role of the electron-electron interaction. Since then, more and more unconventional superconductors have been discovered, chiral superconductors among them.

While the interaction between electrons, the Coulomb interaction, is repulsive, in solids it can give rise to an effective attractive interaction at longer distances while remaining repulsive at the shortest distances. Cooper pairing can exist in a higher angular momentum channel, such as the p -, d - and f - channel, as the higher angular momentum pairing wave functions vanish at short distance.[4] This thesis will focus on chiral superconductivity, a particular type of higher angular momentum pairing.

In this chapter, we briefly summarize some main properties of chiral superconductors. For a detailed review, one can refer to Ref.[5].

1.1 Chiral Superconductivity

In the continuum limit, for a $2D$ chiral superconductor with Cooper pair angular momentum m , the superconducting gap function is described as

$$\Delta(\theta_{\mathbf{k}}) = \Delta_0 \left(\frac{k}{k_F} \right)^{|m|} e^{im\theta_{\mathbf{k}}}, \quad (1.1)$$

where $\theta_{\mathbf{k}}$ is the azimuthal angle of wavevector \mathbf{k} with respect to the x-axis, k_F is the Fermi wave vector, and $m = \pm 1, \pm 2, \pm 3$ for chiral p -, d -, f -wave superconductors, respectively. Chiral superconductors have topological order and can be characterized by a Chern number C which is a topological invariant[6, 7] defined as

$$C = \frac{1}{4\pi} \int d^2k \hat{h} \cdot \left(\partial_{k_x} \hat{h} \times \partial_{k_y} \hat{h} \right) \quad (1.2)$$

where, $\hat{h} = \mathbf{h}/|\mathbf{h}|$ and $\mathbf{h} = \{\text{Re}[\Delta_k], \text{Im}[\Delta_k], \epsilon(k) - \mu\}$; $\epsilon(k) - \mu$ is the single particle dispersion. In the continuum limit, the Cooper pair angular momentum m is equal to the Chern number C . For the simplest chiral p -wave pairing, the chiral order parameter is $\Delta(\theta_{\mathbf{k}}) = \Delta_0(k_x \pm ik_y)/k_F$ according to Eq.(1.1). The corresponding Chern number is ± 1 . These two chiralities, $C = \pm 1$, are degenerate and break time-reversal symmetry. Thus, spontaneous currents are expected at the surfaces or at defects.

The edges and vortices of chiral superconductors can support Majorana zero energy bound states[8, 9], protected by the topology. Majorana zero energy modes carry no electric charge and are represented by a real operator, such that the annihilation and creation operators are identical. These bound states can be potentially used to build a topological quantum computer[10] due to the non-abelian mutual statistics between different vortices carrying the bound states[11].

Several materials are thought to be chiral superconductors in part because experiments suggest a time reversal symmetry broken superconducting phase. Sr_2RuO_4 is a strong candidate for a chiral p -wave superconductor and UPt_3 is thought to have chiral f -wave pairing. SrPtAs and URu_2Si_2 are possible candidates for chiral d -wave superconductors. Among these candidates, Sr_2RuO_4 is the most studied material. The most important evidence for time reversal symmetry breaking comes from μSR [12] and Kerr effect[13] measurements.

1.2 Spontaneous edge current

Another consequence of the time reversal symmetry breaking is the spontaneous edge current. The current is carried by both edge and bulk modes[8]. For chiral superconductors, the edge modes are chiral Majorana-Weyl modes[8, 5]. The number of edge branches is determined by the Chern number defined in Eq.(1.2), which is a manifestation of the bulk-boundary correspondence[14].

The edge current, as well as the related spontaneous angular momentum, in chiral p -wave superconductors/superfluids has been studied extensively[15, 8, 16, 17, 18, 19], partially due to the fact the chiral p -wave is experimentally realized in ^3He [20]. In contrast, similar studies for higher angular momentum chiral superconductors, such

as chiral d -wave[21, 22] and f -wave, are relatively rare. Some of these studies can be found in Ref.[17, 18]. Interestingly, in these studies, the authors have found that the edge current in higher chirality superconductors behaves quite differently from that in chiral p -wave superconductors. However, the conclusions are obtained in the absence of Meissner screening effects.

The Meissner screening effect on the chiral p -wave edge current has been calculated on a half-infinite geometry with a specular surface in Ref.[23]. This study found that the surface magnetic field is largely reduced by the screening effect. However, the effect of screening on higher chirality edge currents has only been studied on a small disk¹ in Ref.[24] recently. Large finite size effects could be induced by the studied geometry. Therefore the question of how the Meissner screening affects the edge current in higher chirality superconductors still needs to be further investigated, i.e., on a half-infinite geometry.

Even though the screened surface magnetic field is reduced by a factor of 10 for the chiral p -wave pairing with parameters appropriate for Sr_2RuO_4 , theoretically it is predicted to be of the order of 10 Gauss[23], which should be observable. However, searches for the expected spontaneous currents in Sr_2RuO_4 have so far yielded null results[25, 26, 27]. One possible reason for the null surface current results is the effect of surface disorder. Experimentally, a specular surface scattering is hard to realize as it requires the superconductor sample surface to be atomically smooth.

Effects of different types of non-specular surfaces, including rough surface, pair breaking surface and metallic surface, has been discussed extensively for chiral p -wave pairing[28, 29, 30, 31, 32, 24, 33]. Only recent studies in Ref.[24] investigated this

¹The geometry studied in Ref.[24] is an infinite cylinder with a small radius comparable to the coherence length.

problem for higher chiral pairings on a small disk. Interestingly, the authors found that the direction of the chiral d -wave edge current is flipped by the surface roughness. Again, this conclusion may suffer from the large finite size effects. Thus, the effects of surface roughness on both the unscreened and screened spontaneous edge current for different chiral pairings are still unclear.

1.3 Plan of this thesis

The goal of this thesis is to investigate the behavior of the spontaneous edge current of higher chirality superconductors. We will study this problem in the quasiclassical limit of the continuum model.

We will first briefly derive the quasiclassical Eilenberger equation from the Gor'kov equation and introduce the framework of the Eilenberger equation in Chapter 2. The uniform order parameter analytical solutions to the Eilenberger equation will also be calculated in this chapter. We then discuss the behavior of the self-consistent edge current for different chiral pairings in the absence of the Meissner effect in Chapter 3. We will focus on two features: the spatial profiles of the edge current and the temperature dependence of the integrated current. In Chapter 4, we will address the effects of Meissner screening on the spontaneous edge current. Finally, in Chapter 5, we will add the roughness near the surface and explain its effects on both the unscreened and screened edge current. Conclusions will be given in Chapter 6. A few of the more mathematical details on the Gor'kov equation are left to Appendix A.

Chapter 2

Quasiclassical Formulation

The response of chiral superconductors to inhomogeneity, of which an edge is one important example, can be studied using standard techniques. From the BCS Hamiltonian and its equation of motion, the Gor'kov equation for the Matsubara Green's functions[34], which is often used to study inhomogeneity in superconductors, can be derived with the mean field approximation and Wick-decomposition. One approach is to solve the Gor'kov equation, supplemented with the gap equation and Maxwell equations, self-consistently and then calculate physical quantities using the Matsubara Green's functions. However, the Gor'kov equation is too complex to solve directly.

The quasiclassical formulation greatly simplifies the Gor'kov equation. The Gor'kov equation is associated with two characteristic length scales: \mathbf{k}_F^{-1} and the coherence length, $\xi \sim \hbar \mathbf{v}_F / \Delta$, where Δ here is the bulk superconducting gap, \mathbf{v}_F is the Fermi velocity and \mathbf{k}_F is the Fermi wave vector. By integrating out energies related to \mathbf{k}_F^{-1} , which are unimportant for superconductivity, the Eilenberger equation for the quasiclassical Green's functions[35, 36] can be derived. One can then solve the simpler

Eilenberger equation instead of the Gor'kov equation. Boundary conditions[37] are also needed, as the Eilenberger equation does not contain the physics at very small length scales, related to \mathbf{k}_F^{-1} .

A large number of studies have been done using this framework [38, 39, 40, 41, 23]. In this chapter, we will give a brief description of this framework starting from the Gor'kov equation. A short derivation of the Gor'kov equation, as well as the definition of the Matsubara Green's Functions, is given in Appendix A. For full mathematical details, one can refer to Ref.[42, 43, 44].

2.1 Quasiclassical Approximation

In Appendix A, we derive the Gor'kov equation, Eq.(A.30), which we reproduce here:

$$\begin{pmatrix} -i\omega_n + H & -\Delta(\mathbf{r}_1) \\ \Delta^*(\mathbf{r}_1) & i\omega_n + H^* \end{pmatrix} \hat{G}(\mathbf{r}_1, \mathbf{r}_2; \omega_n) = \delta(\mathbf{r}_1 - \mathbf{r}_2) \hat{1}, \quad (2.1a)$$

$$\hat{G}(\mathbf{r}_1, \mathbf{r}_2; \omega_n) \begin{pmatrix} -i\omega_n + H^* & -\Delta(\mathbf{r}_2) \\ \Delta^*(\mathbf{r}_2) & +i\omega_n + H \end{pmatrix} = \delta(\mathbf{r}_1 - \mathbf{r}_2) \hat{1}. \quad (2.1b)$$

Where, $\hat{G}(\mathbf{r}_1, \mathbf{r}_2; \omega_n)$ is the matrix form of the Matsubara Green's functions,

$$\hat{G}(\mathbf{r}_1, \mathbf{r}_2; \omega_n) = \begin{pmatrix} G(\mathbf{r}_1, \mathbf{r}_2; \omega_n) & F(\mathbf{r}_1, \mathbf{r}_2; \omega_n) \\ -F^\dagger(\mathbf{r}_1, \mathbf{r}_2; \omega_n) & \bar{G}(\mathbf{r}_1, \mathbf{r}_2; \omega_n) \end{pmatrix}. \quad (2.2)$$

As discussed above, Eq.(2.1) can be simplified by using the quasiclassical approximation. Physical quantities, such as the charge current, are defined by the Green's

functions in the limit of $\mathbf{r}_1 \rightarrow \mathbf{r}_2$. Doing a Fourier transform so that functions of $\mathbf{r} = \mathbf{r}_1 - \mathbf{r}_2$ become functions of momentum \mathbf{p} , we can parameterize the momentum-space integral as:

$$\frac{d^3p}{(2\pi)^3} = \frac{d\xi_{\mathbf{p}}}{v_F} \frac{dS_F}{(2\pi)^3}, \quad (2.3)$$

where $d\xi_{\mathbf{p}}/v_F$ is the integral element perpendicular to the Fermi surface and dS_F is the Fermi surface area element. Note that, the first term on the right hand side of Eq.(2.3) is only associated with the fast oscillations $\sim \mathbf{k}_F^{-1}$, which are unimportant for superconductivity.

The quasiclassical Green's functions are obtained by integrating out $\xi_{\mathbf{p}}$ near the surface and are defined as:

$$f(\hat{\mathbf{p}}_F, \mathbf{k}; \omega_n) = \int \frac{d\xi_{\mathbf{p}}}{i\pi} F(\mathbf{p}, \mathbf{k}; \omega_n) = \oint \frac{d\xi_{\mathbf{p}}}{i\pi} F(\mathbf{p}, \mathbf{k}; \omega_n), \quad (2.4a)$$

$$f^\dagger(\hat{\mathbf{p}}_F, \mathbf{k}; \omega_n) = \int \frac{d\xi_{\mathbf{p}}}{i\pi} F^\dagger(\mathbf{p}, \mathbf{k}; \omega_n) = \oint \frac{d\xi_{\mathbf{p}}}{i\pi} F^\dagger(\mathbf{p}, \mathbf{k}; \omega_n), \quad (2.4b)$$

$$g(\hat{\mathbf{p}}_F, \mathbf{k}; \omega_n) = \int \frac{d\xi_{\mathbf{p}}}{i\pi} G(\mathbf{p}, \mathbf{k}; \omega_n) = \oint \frac{d\xi_{\mathbf{p}}}{i\pi} G(\mathbf{p}, \mathbf{k}; \omega_n), \quad (2.4c)$$

$$\bar{g}(\hat{\mathbf{p}}_F, \mathbf{k}; \omega_n) = \int \frac{d\xi_{\mathbf{p}}}{i\pi} \bar{G}(\mathbf{p}, \mathbf{k}; \omega_n) = \oint \frac{d\xi_{\mathbf{p}}}{i\pi} \bar{G}(\mathbf{p}, \mathbf{k}; \omega_n). \quad (2.4d)$$

Where we have also done a Fourier transform from the variable $\mathbf{R} = (\mathbf{r}_1 + \mathbf{r}_2)/2$ to the momentum variable \mathbf{k} . \oint shows that we take the contributions from poles close to the Fermi surface. $\hat{\mathbf{p}}_F$ is the unit vector of particle momentum at (or close to) the Fermi surface.

The mixed coordinate quasiclassical Green's functions in a matrix form can be

expressed as:

$$\hat{g}(\hat{\mathbf{p}}_F, \mathbf{R}; \omega_n) = \begin{pmatrix} g(\hat{\mathbf{p}}_F, \mathbf{R}; \omega_n) & f(\hat{\mathbf{p}}_F, \mathbf{R}; \omega_n) \\ -f^\dagger(\hat{\mathbf{p}}_F, \mathbf{R}; \omega_n) & \bar{g}(\hat{\mathbf{p}}_F, \mathbf{R}; \omega_n) \end{pmatrix}, \quad (2.5)$$

with the Fourier transformation:

$$\hat{g}(\hat{\mathbf{p}}_F, \mathbf{R}; \omega_n) = \int \frac{d^3k}{(2\pi)^3} e^{i\mathbf{k}\mathbf{R}} \hat{g}(\hat{\mathbf{p}}_F, \mathbf{k}; \omega_n). \quad (2.6)$$

The quasiclassical Green's functions obey particle-hole symmetry in equilibrium and the normalisation condition:

$$g(\hat{\mathbf{p}}_F, \mathbf{R}; \omega_n) + \bar{g}(\hat{\mathbf{p}}_F, \mathbf{R}; \omega_n) = 0; \quad (2.7)$$

$$\hat{g}(\hat{\mathbf{p}}_F, \mathbf{R}; \omega_n) \cdot \hat{g}(\hat{\mathbf{p}}_F, \mathbf{R}; \omega_n) = -\pi^2 \hat{1}. \quad (2.8)$$

With above definitions, the quasiclassical Eilenberger equation can be derived from Eq.(2.1). First, we transform the coordinate variables \mathbf{r}_1 and \mathbf{r}_2 to variables \mathbf{r} and \mathbf{R} and only keep the terms with gradients in \mathbf{r} ,

$$\nabla_{\mathbf{r}_1, \mathbf{r}_2} = \frac{1}{2} \nabla_{\mathbf{R}} \pm \nabla_{\mathbf{r}} = \pm \nabla_{\mathbf{r}}, \quad (2.9a)$$

$$\nabla_{\mathbf{r}_1, \mathbf{r}_2}^2 = \frac{1}{4} \nabla_{\mathbf{R}}^2 \pm \nabla_{\mathbf{R}} \nabla_{\mathbf{r}} + \nabla_{\mathbf{r}}^2 = \pm \nabla_{\mathbf{R}} \nabla_{\mathbf{r}} + \nabla_{\mathbf{r}}^2. \quad (2.9b)$$

The Hamiltonian and order parameter can be expressed as:

$$H_{\mathbf{r}_1, \mathbf{r}_2} = -\frac{\nabla_{\mathbf{r}}^2}{2m} \mp \frac{\nabla_{\mathbf{r}}}{2m} \nabla_{\mathbf{R}} - \mu \mp i \frac{e \nabla_{\mathbf{r}}}{mc} \mathbf{A}(\mathbf{R}); \quad (2.10a)$$

$$\Delta(\mathbf{r}_1, \mathbf{r}_2) = \Delta(\mathbf{R}) \quad (2.10b)$$

The Gor'kov equation can be rewritten in mixed coordinate:

$$\left\{ \left(\begin{array}{cc} -i\omega_n + \frac{e\mathbf{v}_F}{c} \mathbf{A}(\mathbf{R}) & -\Delta(\mathbf{R}) \\ \Delta^*(\mathbf{R}) & i\omega_n - \frac{e\mathbf{v}_F}{c} \mathbf{A}(\mathbf{R}) \end{array} \right) + \left(\xi_p - i \frac{\mathbf{v}_F}{2} \nabla_{\mathbf{R}} \right) \hat{1} \right\} \hat{G}(\mathbf{p}, \mathbf{R}; \omega_n) = \hat{1}, \quad (2.11a)$$

$$\hat{G}(\mathbf{p}, \mathbf{R}; \omega_n) \left\{ \left(\begin{array}{cc} -i\omega_n + \frac{e\mathbf{v}_F}{c} \mathbf{A}(\mathbf{R}) & -\Delta(\mathbf{R}) \\ \Delta^*(\mathbf{R}) & i\omega_n - \frac{e\mathbf{v}_F}{c} \mathbf{A}(\mathbf{R}) \end{array} \right) + \left(\xi_p + i \frac{\mathbf{v}_F}{2} \nabla_{\mathbf{R}} \right) \hat{1} \right\} = \hat{1}. \quad (2.11b)$$

Where, $\xi_p = p^2/2m - \mu$ and the Fourier transformation:

$$\hat{G}(\mathbf{p}, \mathbf{R}; \omega_n) = \int d^3r e^{i\mathbf{p}\cdot\mathbf{r}} \hat{G}(\mathbf{r}, \mathbf{R}; \omega_n) \quad (2.12)$$

Subtracting Eq.(2.11a) and Eq.(2.11b), we can get:

$$-i\mathbf{v}_F \nabla_{\mathbf{R}} \hat{G}(\mathbf{p}, \mathbf{R}; \omega_n) = \left[\left(\begin{array}{cc} i\omega_n - \frac{e\mathbf{v}_F}{c} \mathbf{A}(\mathbf{R}) & \Delta(\mathbf{R}) \\ -\Delta^*(\mathbf{R}) & -i\omega_n + \frac{e\mathbf{v}_F}{c} \mathbf{A}(\mathbf{R}) \end{array} \right), \hat{G}(\mathbf{p}, \mathbf{R}; \omega_n) \right]. \quad (2.13)$$

Note that, in Eq.(2.13), the fast oscillations only exist in G . Integrating out the

$d\xi_p$ in G , we can get the Eilenberger equation:

$$-i\mathbf{v}_F \nabla_{\mathbf{R}} \hat{g}(\hat{\mathbf{p}}_F, \mathbf{R}; \omega_n) = \left[\begin{array}{cc} \left(i\omega_n - \frac{e\mathbf{v}_F}{c} \mathbf{A}(\mathbf{R}) & \Delta(\mathbf{R}) \right) \\ \left(-\Delta^*(\mathbf{R}) & -i\omega_n + \frac{e\mathbf{v}_F}{c} \mathbf{A}(\mathbf{R}) \right) \end{array} \right], \hat{g}(\hat{\mathbf{p}}_F, \mathbf{R}; \omega_n) \quad (2.14)$$

2.2 Numerical Procedure

Consider a semi-infinite geometry with a specular surface perpendicular to the x -direction and superconducting at $x \geq 0$. The classical trajectory of a Bogoliubov quasiparticle is shown in Fig. 2.1. The chiral p -wave pairing in this geometry has been calculated in Ref.[23]. In this thesis, we follow the same numerical procedure.

As the system is translationally invariant perpendicular to the x -axis, the corresponding Eilenberger equation can be expressed as:

$$-iv_{F_x} \frac{d}{dx} g(\mathbf{k}_F, x; \omega_n) = \Delta^*(\mathbf{k}, x) f(\mathbf{k}_F, x; \omega_n) - \Delta(\mathbf{k}_F, x) f^\dagger(\mathbf{k}, x; \omega_n), \quad (2.15a)$$

$$i\tilde{\omega}_n f(\mathbf{k}_F, x; \omega_n) + i\frac{1}{2}v_{F_x} \frac{d}{dx} f(\mathbf{k}_F, x; \omega_n) = \Delta(\mathbf{k}_F, x) g(\mathbf{k}_F, x; \omega_n), \quad (2.15b)$$

$$i\tilde{\omega}_n f^\dagger(\mathbf{k}_F, x; \omega_n) - i\frac{1}{2}v_{F_x} \frac{d}{dx} f^\dagger(\mathbf{k}_F, x; \omega_n) = \Delta^\dagger(\mathbf{k}_F, x) g(\mathbf{k}_F, x; \omega_n), \quad (2.15c)$$

where $\tilde{\omega}_n = \omega_n + i\frac{e v_{F_y}}{c} A_y(x)$.

As we see in Eq.(2.15), the equations for g , f and f^\dagger are coupled with each other, which is difficult to solve directly. Riccati parameterization can decouple the Eilenberger equation into scalar differential equations which are much easier to solve numerically.[38, 45]

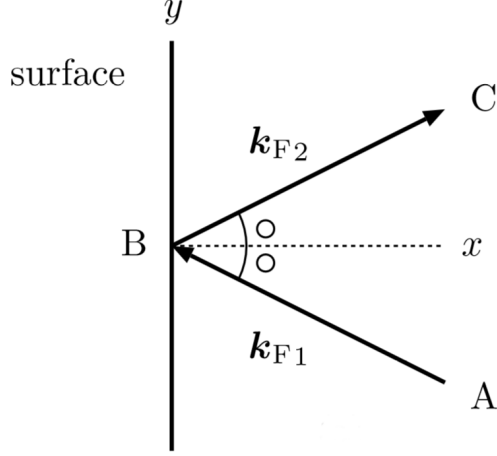


Figure 2.1: Classical trajectory of a Bogoliubov quasiparticle. Adapted from Ref.[23]

The Riccati transformation of the quasiclassical Green's function is defined as:

$$\hat{g} = \frac{-\pi i}{1 + ab} \begin{bmatrix} 1 - ab & 2ia \\ -2ib & -1 + ab \end{bmatrix}. \quad (2.16)$$

Substituting Eq.(2.16) into the Eilenberger equation Eq.(2.15), we get two differential equations for a and b , respectively:

$$v_{F_x} \frac{d}{dx} a(\mathbf{k}_F, x; \omega_n) = \Delta(\mathbf{k}_F, x) - \Delta^\dagger(\mathbf{k}_F, x) a^2(\mathbf{k}_F, x; \omega_n) - 2\tilde{\omega}_n a(\mathbf{k}_F, x; \omega_n), \quad (2.17a)$$

$$v_{F_x} \frac{d}{dx} b(\mathbf{k}_F, x; \omega_n) = -\Delta^\dagger(\mathbf{k}_F, x) + \Delta(\mathbf{k}_F, x) b^2(\mathbf{k}_F, x; \omega_n) + 2\tilde{\omega}_n b(\mathbf{k}_F, x; \omega_n). \quad (2.17b)$$

Note that the differential equations for a and b are no longer coupled to each other and can be solved separately with proper initial values. For $i\omega_n$ situated in the upper half of the complex plane, a can be found by integrating Eq.(2.17a) as an initial value problem along trajectory $A \rightarrow B \rightarrow C$, while b can be found by integrating Eq.(2.17b)

along trajectory $C \rightarrow B \rightarrow A$. [45] The initial values for a and b are

$$a(\mathbf{k}_{F1}, \infty; \omega_n) = \frac{\Delta(\mathbf{k}_{F1}, \infty)}{\sqrt{\omega_n^2 + |\Delta(\mathbf{k}_{F1}, \infty)|^2 + \omega_n}}, \quad (2.18a)$$

$$b(\mathbf{k}_{F2}, \infty; \omega_n) = \frac{\Delta^\dagger(\mathbf{k}_{F2}, \infty)}{\sqrt{\omega_n^2 + |\Delta(\mathbf{k}_{F2}, \infty)|^2 + \omega_n}}, \quad (2.18b)$$

where \mathbf{k}_{F1} and \mathbf{k}_{F2} are the Fermi wave vectors of the incident and reflected quasiparticles as shown in Fig. 2.1. The momentum of the incident and reflected quasiparticles along the surface is conserved and boundary conditions at $x = 0$ are given by:

$$a(\mathbf{k}_{F1}, 0; \omega_n) = a(\mathbf{k}_{F2}, 0; \omega_n), \quad (2.19a)$$

$$b(\mathbf{k}_{F1}, 0; \omega_n) = b(\mathbf{k}_{F2}, 0; \omega_n). \quad (2.19b)$$

For a chiral superconductor with angular momentum m , the order parameter can be separated into two components:

$$\Delta(\mathbf{k}_F, x) = \Delta_x(x) \cos(m\theta_k) + i\Delta_y(x) \sin(m\theta_k). \quad (2.20)$$

The spatial dependent order parameter components can be calculated with the gap equation,

$$\Delta_x(x) = \pi T N(0) V \sum_{|\omega_n| < \omega_C} \frac{1}{2\pi} \int_{-\pi}^{\pi} d\theta_k 2 \cos(m\theta_k) f(\theta_k, x; \omega_m), \quad (2.21a)$$

$$\Delta_y(x) = \pi T N(0) V \sum_{|\omega_n| < \omega_C} \frac{1}{2\pi} \int_{-\pi}^{\pi} d\theta_k 2 \sin(m\theta_k) f(\theta_k, x; \omega_m). \quad (2.21b)$$

Where $N(0)$ is the normal density of states per unit volume at the Fermi energy and $N(0)V$ is the coupling constant determined by:

$$N(0)V = \frac{1}{\ln \frac{T}{T_C} + \sum_{0 < m < \omega_C / 2\pi T} \frac{1}{m-1/2}}. \quad (2.22)$$

Here, T_C is the superconducting transition temperature and ω_C is the cutoff energy.

The spatial dependent current density along y direction can be calculated as,

$$J_y(x) = -ev_F N(0)T \sum_{|\omega_n| < \omega_C} \frac{1}{2\pi} \int_{-\pi}^{\pi} d\theta_k \sin(\theta_k) (-i\pi) g(\theta_k, x; \omega_m). \quad (2.23)$$

The Meissner screening is taken into account through the self-consistent vector potential which can be calculated using the Maxwell equations,

$$B_z(x) = -\mu \int_0^x dx' J_y(x'), \quad (2.24)$$

$$A_y(x) = -\int_x^\infty dx' B_z(x'), \quad (2.25)$$

where μ is the permeability and related to the penetration depth, $\lambda_L = \sqrt{m/e^2\mu n}$, with the density of electrons n .

In summary, for the geometry of Fig. 2.1, the corresponding Eilenberger equation Eq.(2.15) or Riccati equation Eq.(2.17) can be calculated self-consistently using the initial conditions Eq.(2.18), boundary conditions Eq.(2.19), superconducting gap equation Eq.(2.21) and Maxwell equations Eq.(2.25).

2.3 Uniform Order Parameter Analysis

Before we discuss the self-consistent numerical results, we first consider simple cases with uniform order parameter and ignore the vector potential. Quasi-classical Green's function can be calculated analytically in such cases[46, 47, 48, 23, 16, 19].

The quasi-classical Green's function can be rewritten as:

$$\hat{g} = g_1 \hat{\tau}_1 + g_2 \hat{\tau}_2 + g_3 \hat{\tau}_3, \quad (2.26)$$

where, $\hat{\tau}_i$ ($i = 1, 2, 3$) is the Pauli matrix:

$$\hat{\tau}_1 = \begin{pmatrix} 0 & 1 \\ 1 & 0 \end{pmatrix}, \quad \hat{\tau}_2 = \begin{pmatrix} 0 & -i \\ i & 0 \end{pmatrix}, \quad \hat{\tau}_3 = \begin{pmatrix} 1 & 0 \\ 0 & -1 \end{pmatrix}. \quad (2.27)$$

Comparing with the definition of the quasi-classical Green's function Eq.(2.5), we find $\text{Im}(\Delta) \propto g_1$, $\text{Re}(\Delta) \propto g_2$ and $J_y \propto \text{Im}(g_3)$. The Eilenberger equation, Eq.(2.14), can be rewritten as:

$$\frac{d}{dx} \begin{pmatrix} g_1 \\ g_2 \\ g_3 \end{pmatrix} = \frac{2}{v_{Fx}} \begin{pmatrix} 0 & i\omega_n & -i\Delta_x \\ -i\omega_n & 0 & i\Delta_y \\ i\Delta_x & -i\Delta_y & 0 \end{pmatrix} \begin{pmatrix} g_1 \\ g_2 \\ g_3 \end{pmatrix}, \quad (2.28)$$

where, $\Delta(T) = \Delta_x + i\Delta_y$, i.e., for a chiral p -wave superconductor, $\Delta_x = \Delta(T) \cos \theta_k$ and $\Delta_y = \Delta(T) \sin \theta_k$.

Supplemented with the boundary conditions, $\hat{g}(\mathbf{k}_F, 0; \omega_n) = \hat{g}(-\mathbf{k}_F, 0; \omega_n)$, a general solution to Eq.(2.28) can be calculated:

$$g_+(\mathbf{k}_F, x; \omega_n) = \frac{-\pi\Delta_2}{\lambda} \left(1 + \frac{\Delta_1^2}{\omega_n^2 + \Delta_2^2} e^{-2\frac{\lambda}{|v_{Fx}|}x} \right) - i\pi \frac{\omega_n s \Delta_1}{\omega_n^2 + \Delta_2^2} e^{-2\frac{\lambda}{|v_{Fx}|}x}, \quad (2.29a)$$

$$g_-(\mathbf{k}_F, x; \omega_n) = \frac{-\pi\Delta_1}{\lambda} \left(1 - e^{-2\frac{\lambda}{|v_{Fx}|}x} \right), \quad (2.29b)$$

$$g_3(\mathbf{k}_F, x; \omega_n) = \frac{\pi\omega_n}{\lambda} + \frac{\pi}{\lambda} \frac{\omega_n \Delta_1^2}{\omega_n^2 + \Delta_2^2} e^{-2\frac{\lambda}{|v_{Fx}|}x} - i\pi \frac{s\Delta_1\Delta_2}{\omega_n^2 + \Delta_2^2} e^{-2\frac{\lambda}{|v_{Fx}|}x}, \quad (2.29c)$$

where, $\lambda = \sqrt{\omega_n^2 + \Delta^2(T)}$, $s = \text{sgn}(\Delta_1)$. Here, we use Δ_1 , Δ_2 , g_- and g_+ instead of Δ_x , Δ_y , g_1 and g_2 . Δ_1 and Δ_2 represent the components of the order parameter perpendicular and parallel to the surface (i.e., the suppressed and enhanced components); g_- and g_+ represent the suppressed and enhanced Green's function. Take the chiral p-wave superconductor as an example, $\Delta_1 = \Delta_x$, $\Delta_2 = \Delta_y$, $g_+ = g_1$ and $g_- = g_2$.

The spatial dependent current density can be calculated from the imaginary part of g_3 :

$$J_y(x) = \frac{2T}{(2\pi)^d} \sum_{\omega_n} \oint_{\text{F.S.}} \frac{d\mathbf{k}}{|\mathbf{v}_F|} v_{F_y} \text{Im}(g_3(\mathbf{k}, x; \omega_n)). \quad (2.30)$$

The temperature dependent integrated current $I_y(T)$ can be computed with Eq.(2.30)

as:

$$\begin{aligned}
I_y(T) &= \int_0^\infty dx J_y(x) \\
&= -\frac{1}{2(2\pi)^d} \oint_{\text{F.S.}} \frac{d\mathbf{k}}{|\mathbf{v}_F|} v_{F_y} v_{F_x} \Delta_1 \Delta_2 2\pi T \sum_{\omega_n} \frac{1}{\lambda} \frac{1}{\omega_n^2 + \Delta_2^2} \\
&= \frac{1}{(2\pi)^d} \oint_{\text{F.S.}} \frac{d\mathbf{k}}{|\mathbf{v}_F|} v_{F_y} v_{F_x} \Delta_1 \Delta_2 \times \left[\underbrace{\frac{\pi}{2} \frac{1}{|\Delta_1| |\Delta_2|} \tanh\left(\frac{|\Delta_2|}{2T}\right)}_A \right. \\
&\quad \left. - \underbrace{\int_0^\infty dy \frac{1}{\Delta_2^2 \sinh^2 y + \Delta_1^2 \cosh^2 y} \tanh\left(\frac{|\Delta(T)|}{2T} \cosh y\right)}_B \right]. \tag{2.31}
\end{aligned}$$

As is shown in Eq.(2.31), $I_y(T)$ can be separated into two terms denoted as A and B . The integral associated with term A represents the integrated current carried by the edge states and that associated with term B accounts for the integrated current carried by bulk states.

For a chiral p -wave superconductor, the temperature dependent integrated current can be expressed as:

$$\begin{aligned}
I_{y,p\text{-wave}}(T) &= \frac{2mv_F^2}{(2\pi)^2} \int_{-\pi}^{\pi} d\theta_k \sin^2 \theta_k \cos^2 \theta_k \times \left[\underbrace{\frac{\pi}{2|\sin \theta_k| |\cos \theta_k|} \tanh\left(\frac{\Delta_2 |\sin \theta_k|}{2T}\right)}_A \right. \\
&\quad \left. - \underbrace{\int_0^\infty dy \frac{1}{\sin^2 \theta_k \sinh^2 y + \cos^2 \theta_k \cosh^2 y} \tanh\left(\frac{\Delta(T)}{2T} \cosh y\right)}_B \right]. \tag{2.32}
\end{aligned}$$

When $T = 0$, the integrated current can be calculated,

$$I_y(0) = \frac{2mv_F^2}{(2\pi)^2} \int_{-\pi}^{\pi} d\theta_k \sin \theta_k \cos \theta_k \left(\frac{\pi}{2} - \arctan \left(\frac{\sin \theta_k}{\cos \theta_k} \right) \right) = \frac{\epsilon_F}{4\pi}, \quad (2.33)$$

where ϵ_F is the Fermi energy. What's more, when $T = 0$, the integral associated with A is twice that associated with B , indicating the edge states contribution to the integrated current is twice the bulk states contribution. The minus sign indicates the opposite directions of these two contributions. These results, obtained from the uniform order parameter Eilenberger theory, are consistent with that calculated by Stone and Roy using the BdG theory in Ref.[8].

For chiral d - and f -wave superconductors, the temperature dependent integrated currents are:

$$I_{y,d\text{-wave}}(T) = \frac{2mv_F^2}{(2\pi)^2} \int_{-\pi}^{\pi} d\theta_k \sin \theta_k \cos \theta_k \sin 2\theta_k \cos 2\theta_k \times \left[\underbrace{\frac{\pi \tanh \left(\frac{\Delta(T)|\cos 2\theta_k|}{2T} \right)}{2 |\sin 2\theta_k| |\cos 2\theta_k|}}_A - \underbrace{\int_0^{\infty} dy \frac{1}{\cos 2\theta_k \sinh^2 y + \sin 2\theta_k \cosh^2 y} \tanh \left(\frac{\Delta(T)}{2T} \cosh y \right)}_B \right] \quad (2.34)$$

$$= 0$$

$$\begin{aligned}
I_{y,f\text{-wave}}(T) &= \frac{2mv_F^2}{(2\pi)^2} \int_{-\pi}^{\pi} d\theta_k \sin \theta_k \cos \theta_k \sin 3\theta_k \cos 3\theta_k \times \left[\underbrace{\frac{\pi \tanh\left(\frac{\Delta(T)|\sin 3\theta_k|}{2T}\right)}{2 |\sin 3\theta_k| |\cos 3\theta_k|}}_A \right. \\
&\quad \left. - \underbrace{\int_0^{\infty} dy \frac{1}{\sin 3\theta_k \sinh^2 y + \cos 3\theta_k \cosh^2 y} \tanh\left(\frac{\Delta(T)}{2T} \cosh y\right)}_B \right] \\
&= 0
\end{aligned} \tag{2.35}$$

I_y is zero at all T for chiral d - and f -wave superconductors, as well as for other higher chirality superconductors. What's more, both the edge states contribution and the bulk states contribution are zero, as the integrals associated with A and B are zero. These results are consistent with the zero temperature BdG analysis in Ref.[17].

In summary, the uniform order parameter Eilenberger theory shows zero integrated current for higher chiral superconductors at all T , and non-zero integrated current only for chiral p -wave superconductors.

Chapter 3

Self-consistent Edge Current

Without Screening

In this chapter, we discuss the self-consistent edge current for chiral p -, d - and f -wave superconductors without Meissner screening, i.e., we ignore the vector potential. This would be appropriate for a neutral chiral superfluid (although the units would be different and would describe a mass current rather than a charge current). For the superconducting case, understanding the currents without screening provides key insights into the differences between chiral p -wave and higher chirality. We are interested in two features: the spatial profiles of the current density $J_y(x)$ and the temperature dependence of the integrated current, $I_y(T)$, which are calculated using self-consistent numerical solutions to the Eilenberger or Riccati equations as described in Chapter 2.

3.1 Spatial profiles of the current density

We start with the spatial profiles of $J_y(x)$ of chiral p -, d - and f -wave pairing in the limit of $T \rightarrow 0$ ($T = 0.02T_C$). This problem has been studied recently in Ref.[24] at $T = 0.20T_C$. However, the geometry studied there is a small disk which has large finite size effects.

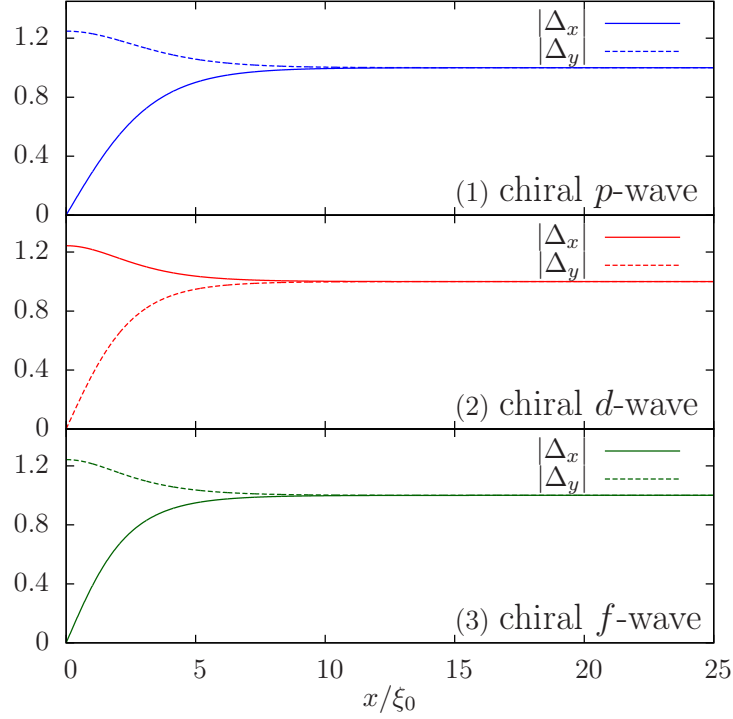


Figure 3.1: Spatial dependence of the self-consistent order parameter components, $|\Delta_x(x)|$ and $|\Delta_y(x)|$, in chiral p - (1), d - (2) and f - (3) wave superconductors without Meissner screening. The x coordinate is scaled by $\xi_0 = v_F/\pi\Delta_0$, where $\Delta_0 = 2\omega_C e^{-1/N(0)V}$ is the magnitude of the bulk order parameter at $T = 0$. The order parameters are scaled by their bulk values. $T = 0.02T_C$. Other parameters used are: the grid size for the θ_k integration is $N_{\theta_k} = 400$ for $\theta_k \in [0, \pi)$; the x -integration grid size is $N_x = 2500$; $\omega_C = 10T_C$ is the Matsubara frequency cutoff. This set of parameters will be used throughout the whole thesis, unless specified otherwise.

Fig. 3.1 shows the spatial profiles of the chiral order parameter components with a specular surface. As can be seen, for all cases, the order parameter components exhibit similar behavior at the edge, i.e., one component drops to zero while the other is slightly enhanced. The component that falls to zero is the one that switches sign under a reflection about the edge. Take the chiral p -wave as an example. Under the reflection $(k_x, k_y) \rightarrow (-k_x, k_y)$, the Δ_x -component changes sign, while the Δ_y -component is invariant. As a consequence, the specular reflection at the edge imposes an effective destructive interference on Δ_x , causing it to vanish at the boundary. The behavior of the other component, which is enhanced, can be understood from the quartic order couplings between the two components.[23]

Fig. 3.2 presents the spatial profiles of the current density, $J_y(x)$, and induced magnetic field, $B_z(x)$, for the three chiral pairings. For chiral p -wave, $J_y(x)$ decays to zero monotonically, inducing a large magnetic field in the bulk, $B_z(x = \infty)$, which indicates a substantial integrated edge current. Nevertheless, $B_z(x = \infty)$ will vanish once the Meissner screening is included, as will be shown in the next chapter. Note that our edge current distribution does not exhibit the characteristic Friedel oscillations generally seen in lattice BdG calculations.[17] This is because the short length scale ($\sim k_F^{-1}$) oscillations have already been integrated out in the Eilenberger formalism.

On the other hand, in agreement with the previous studies[17, 18], the local current density is strongly suppressed for chiral d - and f -wave, as well as for other higher angular momentum chiral pairings (not shown). Furthermore, $J_y(x)$ changes sign from the edge to the bulk. These sign changes lead to the bulk magnetic field, $B_z(x = \infty)$, which is basically zero in Fig. 3.2 ($T = 0.02T_c$), in contrast to the large $B_z(x = \infty)$

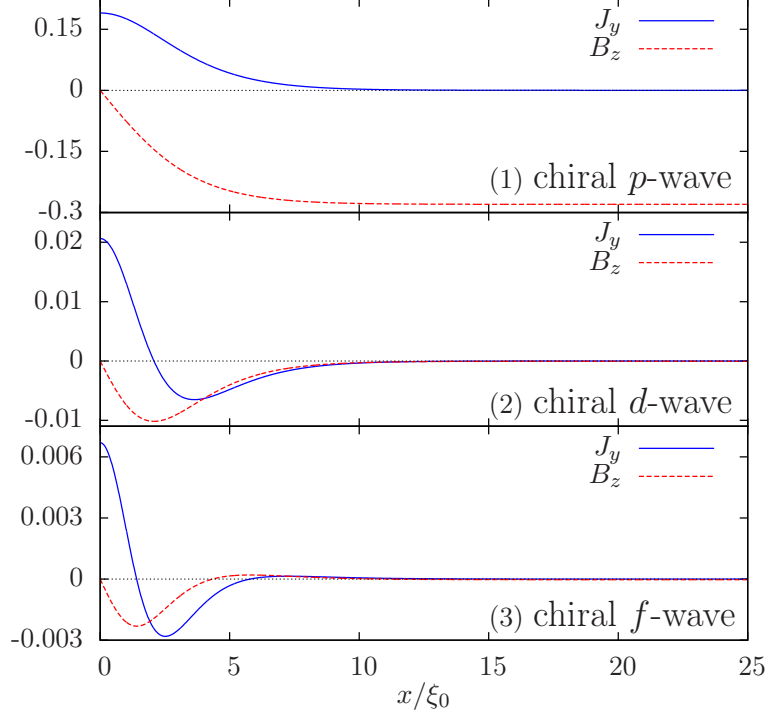


Figure 3.2: Spatial dependence of the current density, $J_y(x)$, and induced magnetic field, $B_z(x)$, in chiral p - (1), d - (2) and f - (3) wave superconductors without Meissner screening. $J_y(x)$ is scaled by $J_0 = ev_F N(0)T_C$ and $B_z(x)$ is scaled by $B_C = \Phi_0/2\sqrt{2}\pi e\xi_0\lambda_L$. $T = 0.02T_C$.

in the p -wave case. At $T = 0$, $B_z(x = \infty)$ should be exactly zero for the chiral d - and f -wave, in accord with our previous analytical integrated current results in Section 2.3.

The suppression and spatial profile of J_y for higher chirality superconductors can be understood from different current channels. In a chiral superconductor, the number of edge branches per edge is determined by the chirality. The current carried by an edge state is proportional to k_y . Thus, the direction, the magnitude and the decay length (in units of the coherence length) of the current density carried by a branch of edge states only depend on the wavevectors. For example, in the chiral d -wave

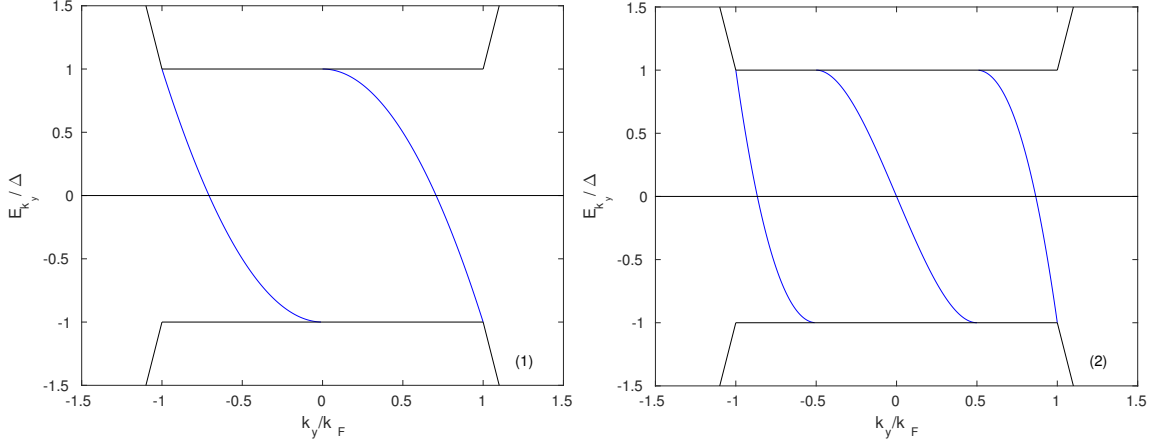


Figure 3.3: Schematic edge dispersion for chiral d - (1) and f - (2) wave superconductor with one edge.

case, there are two edge branches, as is shown in Fig.3.3 (1). The left branch carries negative current and the right branch carries positive current. The current density carried by each branch for $T \approx 0$ is shown in Fig.3.4 (a.1) and (a.2). The negative current channel with $|k_y/k_F| < \sqrt{2}/2$ has a longer decay length; while the positive one with $|k_y/k_F| \geq \sqrt{2}/2$ has a shorter decay length. Because of the cancelation between the two branches the total local current density is largely reduced. Also due to the different length scales of the two channels the local current has a node. Note that in each edge mode branch in Fig.3.3, a Bogoliubov quasiparticle state with momentum k_y is an equal weight combination of normal state electron with momentum k_y and hole with momentum $-k_y$. As a consequence, the current density carried by the k_y edge state in Fig. 3.3 is split into two parts in the Eilenberger formalism: $J_y(k_y)$ (electron like) and $J_y(-k_y)$ (hole like), which explains why in Fig.3.4 the positive current branch is nonzero for both $k_y > 0$ and $k_y < 0$. Similarly, in a chiral f -wave superconductor with one edge, three current channels carrying current density on three different length scales account for the suppression and the spatial profiles of the

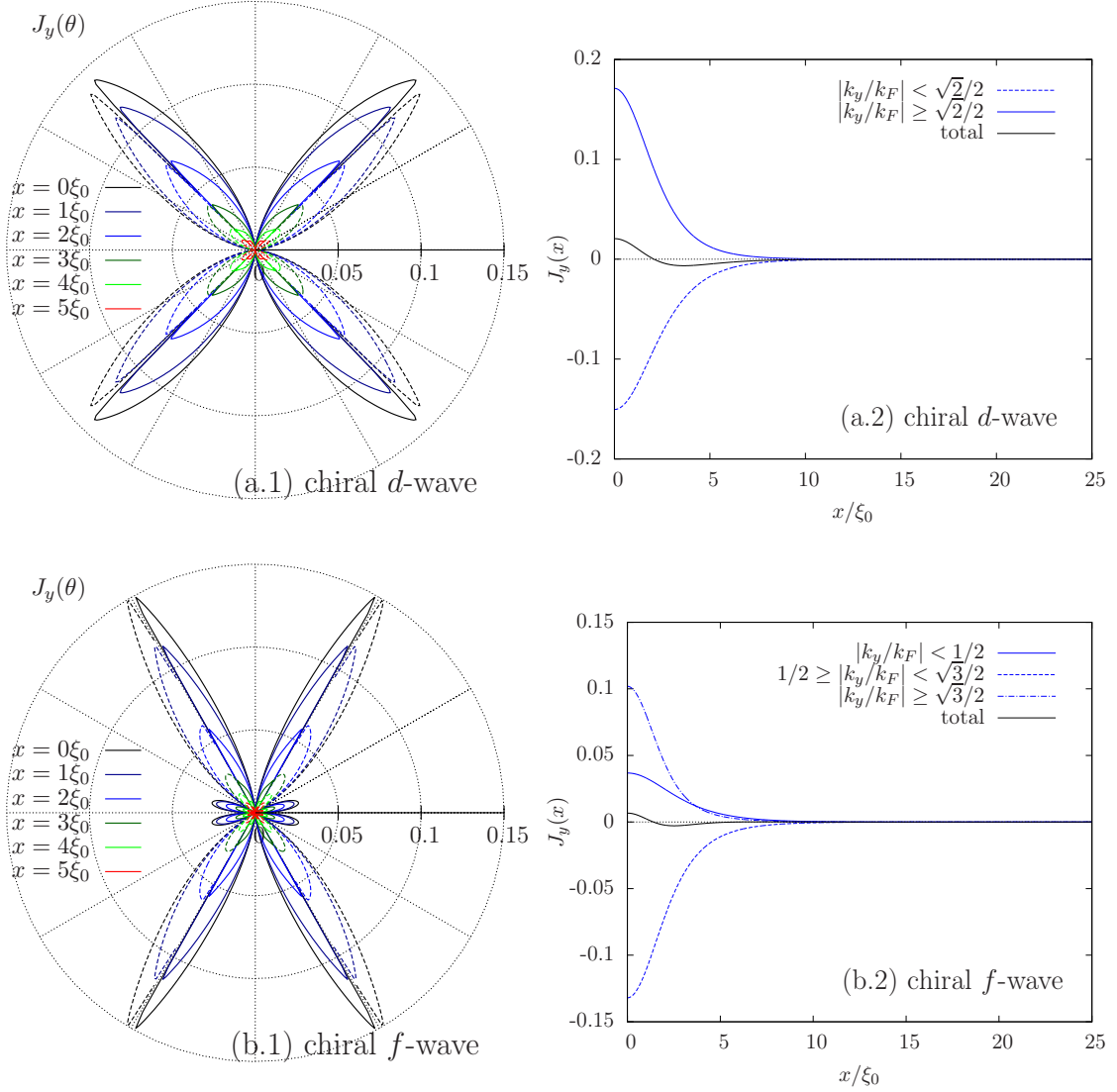


Figure 3.4: Angular dependence of $J_y(\theta)$ at several positions and spatial dependence of $J_y(x)$ in different channels for chiral d - (a) and f - (b) wave superconductors without screening. In (a.1) and (b.1), the solid lines represent positive current density and dash lines represent negative current density. $T = 0.02T_C$.

local current density.

It is important to note that, on the basis of a phenomenological Ginzburg-Landau argument, Ref.[17] predicts vanishing local edge current for non- p -wave chiral superconductors. However, both Ref.[24] and our calculations indicate finite, albeit small, local current distribution. This need not constitute a serious inconsistency as the Ginzburg-Landau analysis in Ref.[17] only takes into account the lowest order contributions, namely,

$$J_y \propto k_3 \text{Im}[(\partial_x \Delta_x^*) \Delta_y - \Delta_x^* (\partial_x \Delta_y)] \quad (3.1)$$

There, the expectation of vanishing local current stems from the symmetry of the phenomenological coefficient k_3 , which vanishes for non- p -wave chiral pairings. However, higher order contributions, such as $(\partial_x^3 \Delta_x^*) \Delta_y$, may not vanish, thus leading to non-zero local current distribution.

3.2 Temperature dependence of the integrated current

As discussed in Sec.2.3, when the order parameter is uniform, $I_y(T)$ is zero for higher chirality pairings at all T ; however, it is substantial for chiral p -wave at $T = 0$. Here we discuss the self-consistent $I_y(T)$ for different chiral pairings.

For the chiral p -wave pairing, the uniform order parameter analysis predicts $I_{y,analytical}(0) = \epsilon_F/4\pi$. For the convenience of comparison with the numerical results, we scale the integrated current by $I_0 = J_0 \xi_0 = ev_F N(0) T_C \xi_0$ and get $I_{y,analytical}(0)/I_0 =$

0.722. The numerical results, with both uniform order parameter and self-consistent spatial varying order parameter, are in agreement with the analytical solution in the limit of $T \rightarrow 0$, $N_x \rightarrow \infty$ and $\omega_C \rightarrow \infty$ ¹. Fig. 3.5 shows the self-consistent $I_y(T)/I_y(0)$ compared with the uniform non-self-consistent numerical results and the uniform analytical solutions. As can be seen, the non-self-consistent results are in agreement with the analytical solutions at all temperatures, as expected. However, $I_y(T)$ is sensitive to the details of the order parameter at the edge (i.e., to self-consistency) at finite temperature.

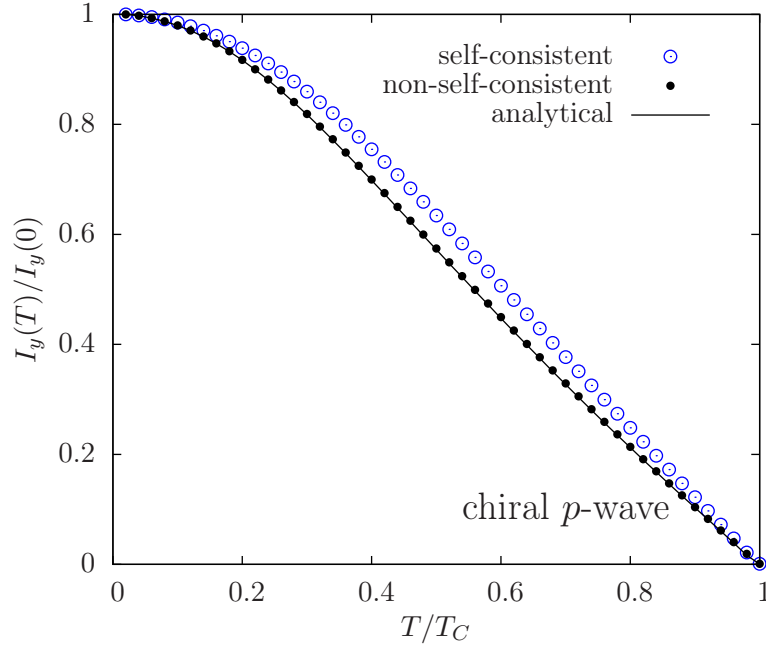


Figure 3.5: Temperature dependence of the self-consistent $I_y(T)/I_y(0)$ (open circles) for chiral p -wave pairing compared with the uniform non-self-consistent numerical results (solid circles) and the uniform analytical solution (line). As we don't have the numerical results at $T = 0$, we use $I_y(T)/I_y(0.02T_C)$ instead. $\omega_C = 20T_C$

For the chiral d - and f -wave pairing, the numerical results, both with and without

¹With parameters chosen as $N_x = 2500$ and $\omega_C = 20T_C$, $I_{y,\text{self}}(0.02T_C)/I_0 = 0.691$.

self-consistency, are in agreement with the analytical solution in the limit of $T \rightarrow 0$, $N_x \rightarrow \infty$ and $\omega_C \rightarrow \infty$, that is $I_{y,\text{analytical}}(0) = I_{y,\text{self}}(0) = I_{y,\text{non-self}}(0) = 0$. As shown in Fig. 3.6, both the uniform non-self-consistent numerical results and the analytical solutions give $I_y = 0$ at all temperatures. However, with self-consistency, $I_y(T)$ is non-zero at $T > 0$.

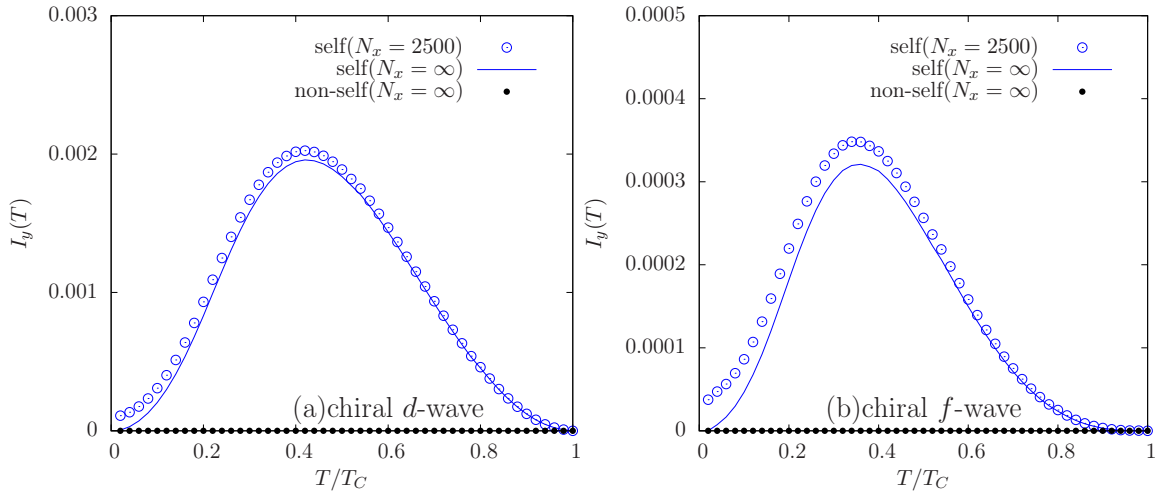


Figure 3.6: Temperature dependence of the self-consistent current $I_y(T)$ (open circles) compared with the uniform non-self-consistent numerical results (solid circles) for chiral d -wave (a) and chiral f -wave (b). The $N_x = \infty$ data is obtained from results of finite N_x by extrapolation to reduce the finite size effects. $\omega_C = 20T_C$.

The difference between the self-consistent and the uniform or non-self-consistent $I_y(T)$ at $T > 0$ for the three chiral pairings can be understood as resulting from the change in the edge dispersions with self-consistency. As mentioned earlier and from the analytical analysis in Ref.[49], the current carried by an edge state is proportional to k_y and the current from edge states between k_y to $k_y + dk_y$ is proportional to $k_y dk_y$. Self-consistency slightly modifies the edge dispersion; however $E_{k_y} = 0$ points are protected by the pairing symmetry: for chiral p -wave, $E_{k_y} = 0$ at $k_y = 0$, while for chiral d -wave, $E_{k_y} = 0$ at $k_y = \pm\sqrt{2}/2$. As a consequence, in the ground state of

chiral superconductors, the self-consistent $I_y(0)$ is equal to the uniform $I_y(0)$, since the same k_y -states are occupied in the two cases and the current carried by a state only depends on k_y and not the energy of the state (i.e., there is no dependence on the dispersion). However, when $T > 0$, some states with $E_{k_y} > 0$ will be occupied while some states with $E_{k_y} < 0$ will be empty and the thermal occupation of any state depends on its energy, i.e., is dependent on the dispersion which is affected by self-consistency. Consequently, $I_y(T)$ depends on the details of the edge dispersion.

In summary, the multiple current channels in higher chirality superconductors result in the suppression of the local current density and the presence of nodes in the current spatial profiles. Self-consistency induces spatial varying order parameters which slightly modifies the $E_k \neq 0$ edge dispersion. As a result, the integrated current at $T > 0$ is affected and becomes non-zero in the case of higher chirality.

Chapter 4

Self-consistent Edge Current With Screening

In this chapter, we discuss the Meissner screening effect on the edge current for chiral p -, d - and f -wave pairings, i.e., including the self-consistent vector potential A_y induced by the edge current. The chiral p -wave case has been well studied in Ref.[23] and we present the results for the sake of comparison between chiral p -wave and higher chirality cases.

According to Eq.(2.14), $i\omega$ is replaced by $i\omega - \frac{ev_{Fy}}{c}A_y$, when A_y is included in the theory. Quasiparticles moving parallel to the surface are strongly affected by A_y due to the factor v_{Fy} ; by contrast, quasiparticles moving perpendicular to the surface are hardly affected. The spatial varying profiles of the chiral order parameter components near the edge are caused by the quasiparticles moving almost perpendicular to the surface which are weakly affected by the Meissner screening. Consequently, as is shown in Fig. 4.1, the self-consistent order parameters with screening exhibit qualitatively the same spatial profiles as the unscreened results in Fig. 3.1.

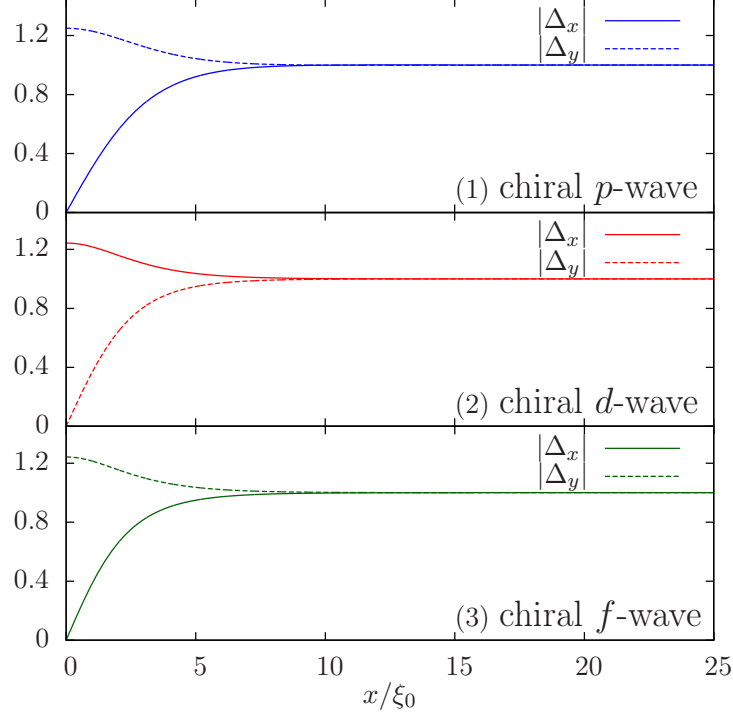


Figure 4.1: Spatial dependence of the self-consistent order parameter components, $|\Delta_x(x)|$ and $|\Delta_y(x)|$, in chiral p - (1), d - (2) and f - (3) wave superconductors with Meissner screening. $T = 0.02T_C$.

The total current density with Meissner screening consists of two terms: paramagnetic current density, $J_{y,\text{para}}(x)$, and diamagnetic current density, $J_{y,\text{dia}}(x)$:

$$J_y(x) = J_{y,\text{para}}(x) + J_{y,\text{dia}}(x), \quad (4.1)$$

satisfying $I_{y,\text{para}} + I_{y,\text{dia}} = 0$. $J_{y,\text{para}}(x)$ is basically the edge current calculated in Chapter 3; however, small changes are expected due to the effect of A_y on the bound states. $J_{y,\text{dia}}(x)$ can be expressed as:

$$J_{y,\text{dia}}(x) = -\frac{e^2 n_s}{mc} A_y(x). \quad (4.2)$$

Eq.(4.2) shows that the induced $J_{y,\text{dia}}(x)$ essentially depends only on the self-consistent $A_y(x)$ because the superfluid density, n_s , is basically position independent for the specular surface case. Recalling the Maxwell equations, Eq.(2.25), $A_y(x)$ can be expressed as:

$$A_y(x) = \frac{m}{e^2 n \lambda_L^2} \int_x^\infty dx' \int_0^{x'} dx'' J_y(x''). \quad (4.3)$$

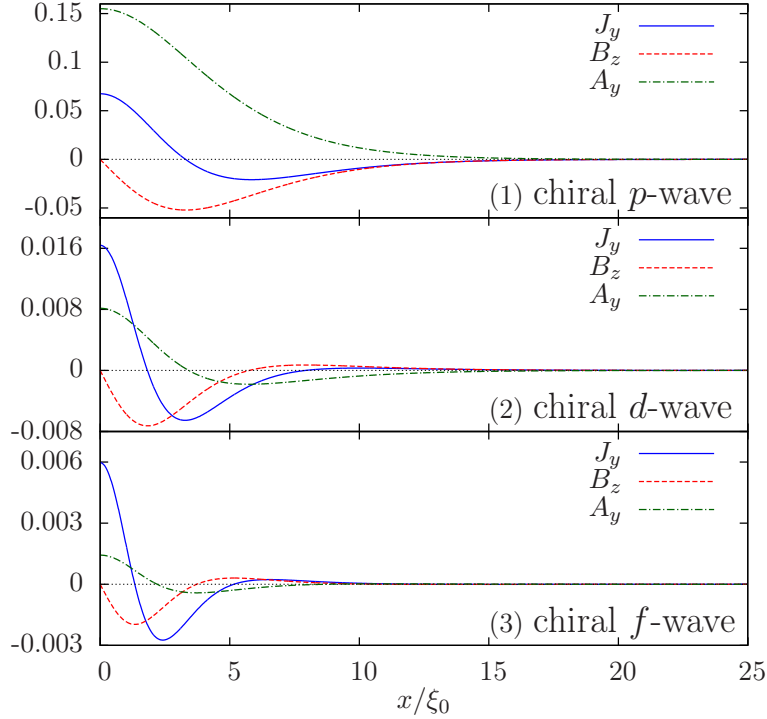


Figure 4.2: Spatial dependence of the self-consistent current density, $J_y(x)$, magnetic field, $B_z(x)$, and vector potential, $A_y(x)$, for chiral p - (1), d - (2) and f - (3) wave superconductors. $T = 0.02T_C$.

Fig. 4.2 shows the spatial dependence of the self-consistent current density, $J_y(x)$, magnetic field, $B_z(x)$, and vector potential, $A_y(x)$, for the three chiral pairings. As can be seen, $J_y(x)$ is reduced by the induced diamagnetic current compared to the un-screened results. As a consequence, the bulk magnetic field, $B_z(x = \infty)$, is screened;

the surface magnetic field is somewhat reduced. What's more, $J_y(x)$, $B_z(x)$ and $A_y(x)$ vary on a longer length, than in the unscreened case, in units of the penetration depth λ_L .

The effect of Meissner screening on higher angular momentum pairings is not as significant as on chiral p -wave case. For chiral p -wave pairing, the unscreened $B_z(x = \infty)$ is large, indicating a large unscreened $I_{y,\text{para}}$. The induced $I_{y,\text{dia}}$ needs to be large as well to compensate $I_{y,\text{para}}$. As a consequence, the surface magnetic field is largely reduced, i.e., $|B_z(x)|_{\text{max}}$ is reduced by 80%. For higher angular momentum pairings, the unscreened $B_z(x = \infty)$ is tiny and, in fact, vanishes at $T = 0$, as discussed in Chapter 3. For chiral d -wave pairing at $T = 0.02T_C$, $|B_z(x)|_{\text{max}}$ is reduced by 30%. Furthermore, the more sign changes in the spatial profiles of J_y , the smaller A_y is (from the double integral in Eq 4.3), resulting in an even smaller reduction; i.e., $|B_z(x)|_{\text{max}}$ is reduced by only 15% for chiral f -wave pairing at $T = 0.02T_C$. Notice, the surface magnetic field is somewhat reduced even in the limit of $T \rightarrow 0$ for higher chiral pairings where the unscreened $B_z(x = \infty) = 0$. The magnitude of the reduction is also affected by λ_L , that is, when λ_L is smaller, the magnitude of the reduction will be larger for all three pairings.

In addition, $J_{y,\text{para}}$ and $J_{y,\text{dia}}$ decay on two different lengths, resulting in an additional sign change in the spatial profiles of the screened $J_y(x)$ for the three chiral pairings. As can be seen when comparing Fig. 4.2 to Fig. 3.2, the difference between the screened and unscreened $J_y(x)$ spatial profiles is significant for the chiral p -wave case. By contrast the additional sign change is barely seen for higher angular momentum cases.

In Fig. 4.3, we show the angular dependence of the total current density $J_y(\theta)$

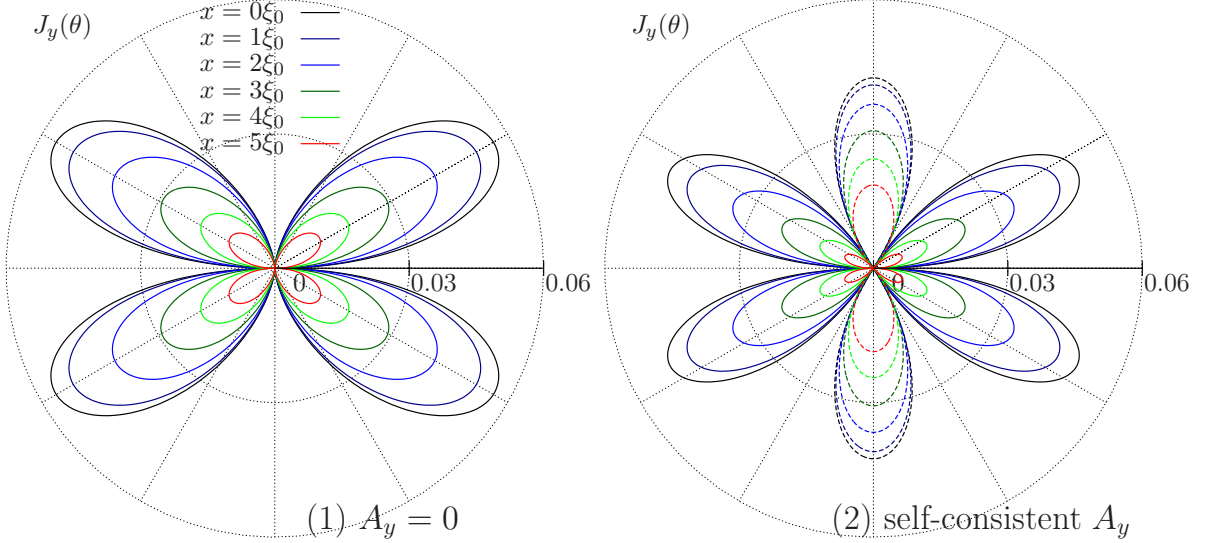


Figure 4.3: Angular dependence of $J_y(\theta)$ at several different positions for chiral p -wave without (1) and with screening (2). The solid lines represent positive current density and dash lines represent negative current density. $T = 0.02T_C$.

for chiral p -wave pairing both without, Fig. 4.3 (1), and with, Fig. 4.3 (2), screening. The solid lines represent positive current density and dash lines represent negative current density. Comparing with the unscreened $J_y(\theta)$ in Fig. 4.3 (1), we see that the negative current density near large $|k_y|$ angles, is primarily from the diamagnetic current density, and the positive current near small $|k_y|$ angles in Fig. 4.3 (2) is basically the paramagnetic current density. However, $J_{y,\text{papa}}(\theta)$ and $J_{y,\text{dia}}(\theta)$ overlap and cancel with each other, especially near $|k_y| = \sqrt{2}/2$. The induced diamagnetic current density in chiral d - and f -wave is tiny compared with the magnitude of the paramagnetic current density of each channel (not shown).

In summary, unlike in the case of chiral p -wave superconductors, Meissner screening is of less importance in higher chirality superconductors with a specular surface, except for cancelling a small a residual bulk field at $T > 0$. It is reasonable to use the

unscreened current as an approximation for chiral d - and f -wave superconductors.

Chapter 5

Rough Surface Effect

As no spontaneous chiral edge currents have been observed experimentally and the edge currents are affected by surface disorder, in this chapter, we study the effect of a rough surface on the edge current for different chiral pairings. To begin, we discuss the unscreened case. A similar calculation has been studied for chiral p -wave pairing in Ref.[33]. We present the chiral p -wave results for comparison. Then we include the Meissner screening and discuss the rough surface effect on the screened edge currents.

We model the rough surface by adding a self-energy due to impurities[50, 24] in the rough surface regime,

$$\hat{\Sigma}(x; \omega_n) = \frac{i}{2\tau_0} \int \frac{d\theta_k}{2\pi} \hat{g}(\theta_k, x; \omega_n), \quad (5.1)$$

to the Hamiltonian in the Eilenberger equation formalism. τ_0 is the mean free time. The mean free path is $l = v_F \tau_0$. The strength of roughness is characterized by ξ_0/l . The simplest way to properly model the rough surface is to assume a constant τ_0

within the regime from $x = 0$ to $x = W$ close to the surface and terminate the rough regime abruptly at $x = W$ [24]. However, this would induce artificial effects near the sharp interface. To avoid this artificial effect we consider a spatial dependent mean free time $\tau(x)$ that varies smoothly from the edge to the bulk. $\tau(x)$ is defined as:

$$\frac{1}{\tau(x)} = \frac{1}{\tau(0)} \times \left(\frac{1 - \tanh(x - W)}{2} \right). \quad (5.2)$$

The corresponding Eilenberger equation can be expressed as:

$$-iv_{F_x} \frac{d}{dx} \hat{g}(\mathbf{k}_F, x; \omega_n) = \left[\hat{H}(\mathbf{k}_F, x; \omega_n) + \hat{\Sigma}(x; \omega_n), \hat{g}(\mathbf{k}_F, x; \omega_n) \right], \quad (5.3)$$

where,
$$\hat{H}(\mathbf{k}_F, x; \omega_n) = \begin{pmatrix} i\omega_n - \frac{ev_{F_y}}{c} A_y(x) & \Delta(x) \\ -\Delta^*(x) & -i\omega_n + \frac{ev_{F_y}}{c} A_y(x) \end{pmatrix}.$$

To start with, a weak roughness, $\xi_0/l = 0.1$, is considered and the Meissner screening is ignored. The spatial profiles of the self-consistent order parameters and $J_y(x)$, compared with the specular surface results (black lines), are shown in Fig. 5.1. As can be seen, both of the chiral order parameter components and $J_y(x)$ are somewhat reduced by the disorder for the three pairings. However, the effects on I_y for different chiralities are different. For chiral p -wave pairing, the suppressed $J_y(x)$ results in a smaller I_y . For higher angular momentum pairings, the current density consists of multiple current channels and the channels carrying current density that vary on a shorter length are more sensitive to the surface effect. For chiral d -wave pairing, the positive current channel is more sensitive to the surface disorder due to the shorter decay length, while, the negative current channel is less sensitive. As a consequence, the positive current channel is suppressed more significantly, resulting in a negative

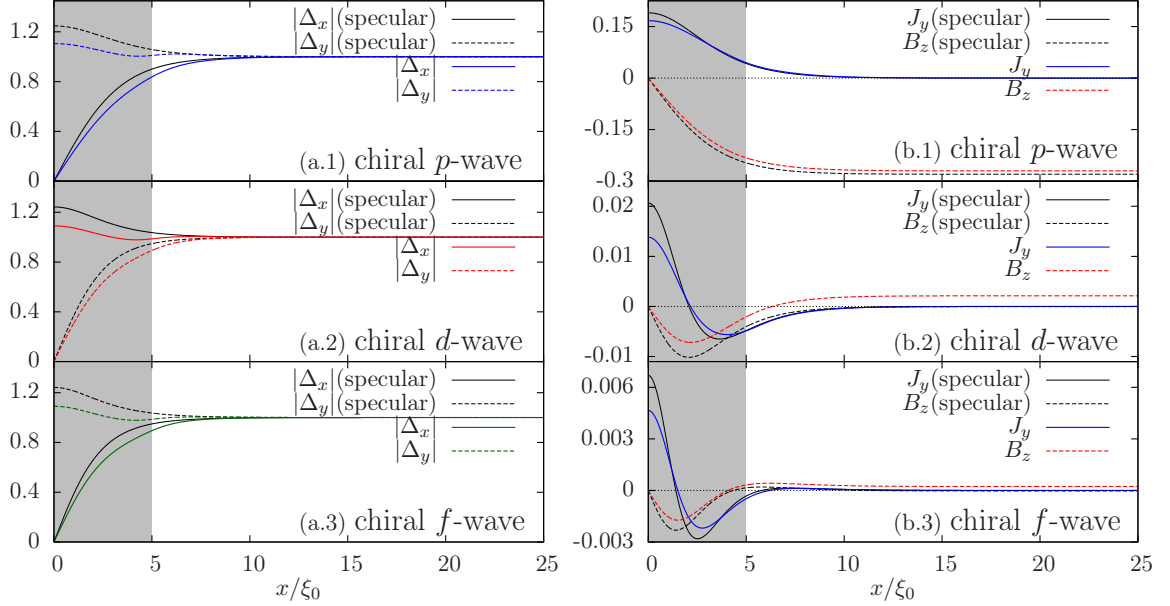


Figure 5.1: (a) Spatial dependence of self-consistent order parameters for chiral p - (a.1), d - (a.2) and f - (a.3) wave pairing with a rough surface. (b) Spatial dependence of self-consistent $J_y(x)$ and $B_z(x)$ for different chiral pairings with a rough surface. $W = 5\xi_0$, $\xi_0/l = 0.1$, $T = 0.02T_C$. The numerical results for the specular surface (black lines) are shown for comparison.

I_y . Similarly, for chiral f -wave pairing, I_y is negative as the current channel that varies on the shortest length carries positive current density.

Superconductivity is largely suppressed in the rough surface regime when stronger surface roughness, $\xi_0/l = 1.0$, is present. As can be seen in Fig. 5.2, the two order parameter components are suppressed to zero at the edge. However, the spatial profiles of $J_y(x)$ exhibit different properties for different pairings. For chiral p -wave pairing, the strong surface roughness further suppresses the edge current, i.e., $|J_y|_{\max}$ is reduced by 35%. For chiral d -wave pairing, the strong roughness inverts the edge current, i.e., $J_y(W) < 0$. What's more, $|J_y|_{\max}$ is larger than the specular surface result. In addition, $|J_y(x > W)|$ decays from the interface to the bulk monotonically, indicating only one current channel exists, instead of two. For chiral f -wave pairing,

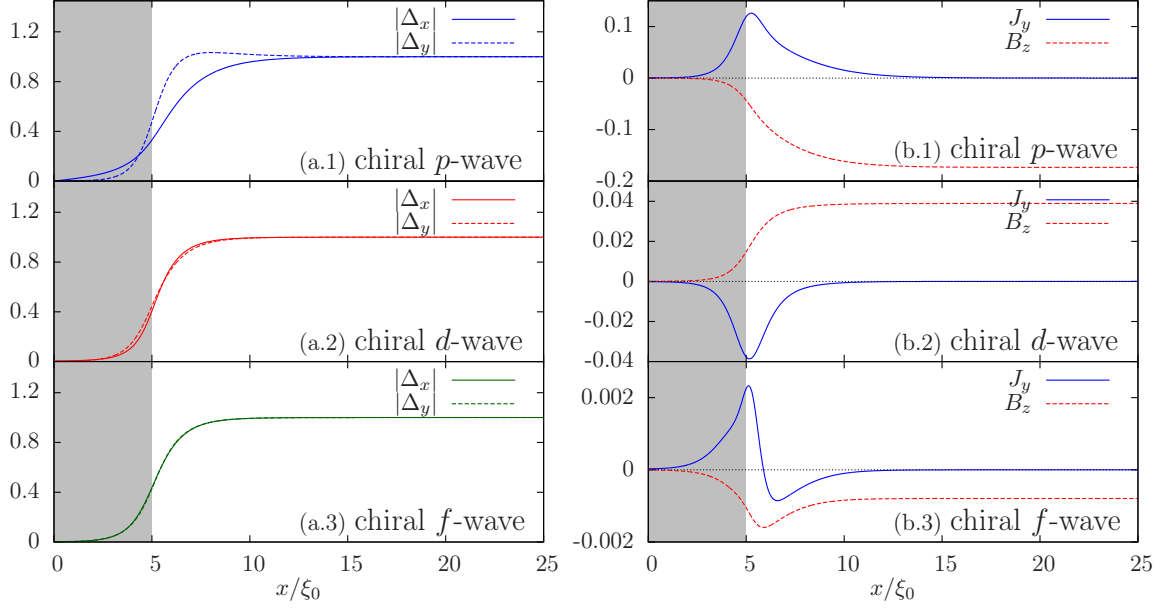


Figure 5.2: (a) Spatial dependence of the self-consistent order parameters for chiral p - (a.1), d - (a.2) and f - (a.3) wave pairing with a rough surface. (b) Spatial dependence of self-consistent $J_y(x)$ and $B_z(x)$ for different chiral pairings with a rough surface. $W = 5\xi_0$, $\xi_0/l = 1.0$, $T = 0.02T_C$.

the edge current is reduced, and no current inversion happens; however, it consists of two current channels instead of three.

The behaviors of the edge current for higher chirality superconductors can be understood with the effects of sub-dominant order parameters. For chiral superconductors, the surface breaks the inversion symmetry and induces sub-dominant order parameters. For example, in a d -wave superconductor, the surface induces an s -wave component which is less sensitive to the disorder. Furthermore, the s -wave component combined with the id_{xy} component, $s + id_{xy}$ pairing, breaks time reversal symmetry and supports edge currents[46, 47, 48, 21, 22]. When a strong rough surface is induced, the chiral order parameter components are largely suppressed, especially the $d_{x^2-y^2}$ component; however, the s -wave component isn't. As a consequence, the edge

current of $s + id_{xy}$ pairing dominates. Specifically, this current is negative in our case as we get a positive s -wave component and a positive id_{xy} component. Similarly, for a chiral f -wave superconductor, the edge current of $f_{x^3-3xy^2} + ip_y$ pairing dominates as the sub-dominant order parameter ip_y , induced by the surface, is less sensitive to the disorder. In general, higher chirality superconductors with odd pairing symmetries are mostly affected by an ip_y component and those with even pairing symmetries are affected by an s -wave component. The effects of sub-dominant order parameters are unimportant in chiral p -wave superconductors.

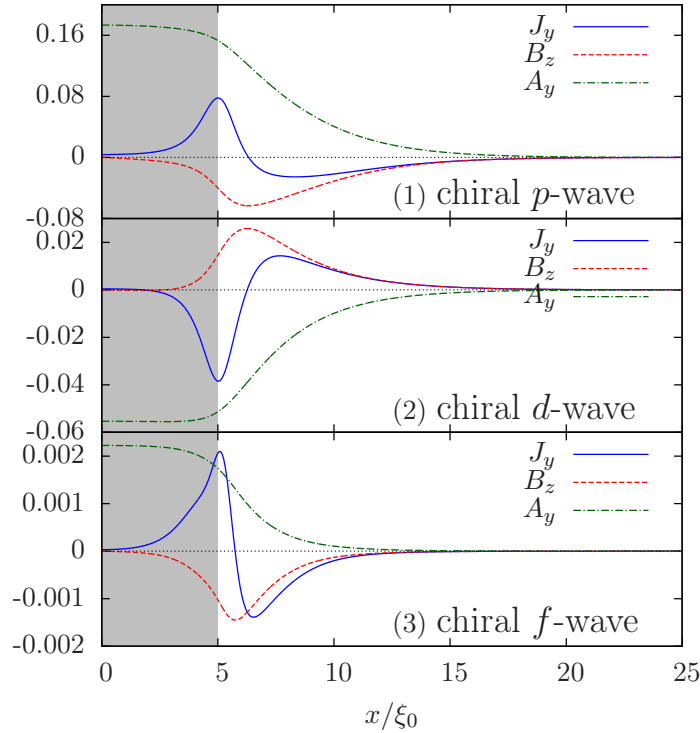


Figure 5.3: Spatial dependence of the self-consistent $J_y(x)$, $B_z(x)$ and $A_y(x)$ for chiral p - (1), d - (2) and f - (3) wave pairing with screening. $W = 5\xi_0$, $\xi_0/l = 1.0$, $T = 0.02T_C$.

We now include the Meissner screening. As we can see in Fig. 5.3, $J_y(x)$ exhibits similar spatial profiles for all three chiral pairings; that is: $|J_y(x)|$ decays to zero

with a sign change from the interface into the bulk. However, $J_y(W)$ is negative for chiral d -wave case, as well as for other even angular momentum chiral pairings (not shown). The universal behavior of $J_y(x)$ is due to the sub-dominant order parameters, specifically, an s -wave component in even angular momentum chiral pairings and an ip_y component in odd angular momentum chiral pairings.

In summary, both the chiral order parameter components and the spontaneous edge current are suppressed by the rough surface when the roughness is weak. However, the sub-dominant order parameters become important for higher chirality superconductors when the roughness is strong enough to suppress both chiral order parameter components to zero.

Chapter 6

Conclusions

To summarize, in this thesis, we have studied the spontaneous edge currents in higher chirality superconductors.

We first investigated the spontaneous edge current in the absence of the Meissner screening. Consistent with Ref.[17, 18], we found that the edge currents of higher chirality pairings are much smaller than for chiral p -wave. In a chiral superconductor with chirality m , the edge current consists of m different channels. The currents carried by different channels have different signs and decay lengths. When $m \neq 1$, they tend to cancel each other, resulting in nodes in the spatial profiles; while in the $m = 1$ case, the cancellations and nodes do not exist. The total integrated current is substantial for chiral p -wave superconductors at $T = 0$ while it vanishes for higher chirality cases at all T when the order parameter is taken to be uniform. This numerical conclusion is exactly in agreement with the non-self-consistent (uniform order parameter) Eilenberger results and also previous studies[17, 18].

Interestingly, when the order parameter is calculated self-consistently and varies near the edge, these conclusions still hold at $T = 0$. However, the integrated current

is non-zero even for higher chirality superconductors at finite T ($0 < T < T_c$). These results can be understood with the self-consistent edge state energy dispersions. The dispersions with energy $E_{k_y} \neq 0$ are slightly modified by the self-consistency compared with the uniform order parameter case. This change affects the behavior of the edge current at finite T . However, the $E_{k_y} = 0$ points, which determine the quasiparticle ground state occupations and therefore the integrated current at $T = 0$, are protected by the pairing symmetry and remain invariant.

We then studied the Meissner effect on the spontaneous edge current. The spatial profiles of the screened edge currents have an additional node compared with the unscreened cases, as the diamagnetic current is governed by the penetration depth, which is taken to be longer than the coherence length. The magnetic field due to the spontaneous edge current is screened to zero in the bulk; the magnetic field near the surface is somewhat reduced for all three chiral pairings. However, the Meissner effects in the higher chirality cases are much weaker than in the chiral p -wave case. As a result, the unscreened edge current is a good approximation to the screened one for higher chirality cases.

Finally, we have discussed the effect of surface roughness. The edge currents are reduced by weak surface roughness for all three chiral pairings in a similar way. However, for stronger roughness, the behaviors of the even chiral pairing edge currents are different from the odd cases for both unscreened and screened cases. The direction of the spontaneous edge current of even chirality pairings is inverted by the strong roughness due to effects of sub-dominant order parameters. Surfaces can break the inversion symmetry and induce sub-dominant order parameters. In higher chirality superconductors, the sub-dominant orders are less sensitive to the disorder and can

survive with the strong roughness; however, the two chiral order parameter components are substantially suppressed, especially the component that is enhanced in the specular surface case. Specifically, the edge current of all odd angular momentum chiral pairings is affected by an ip_y component and all the even pairings are impacted by an s -wave component.

The effects of a strong surface roughness are obtained by considering the surface disorder as a simple 1D self-energy, which is in an approximation to isotropic elastic scattering. Future studies with more realistic disorder models are needed to fully understand of rough surface effects. However, such disorders are difficult to model in the quasiclassical limit. Instead of quasiclassical Eilenberger equations, Bogoliubov-de Gennes equations for a lattice model is a good formalism for studying a system with impurities, although the system sizes one can study is limited. A similar calculation on a 2D square lattice with a metallic surface for chiral p -wave pairing has been studied in Ref.[32]. Rough surface effects on the edge current of higher angular momentum chiral pairings, such as chiral d - and f -wave pairings, can be calculated on a triangular lattice with impurities near the edge.

Appendix A

Gor'kov Equation for Matsubara Green's Functions

For a full description of the quasiclassical approach, we briefly derive the Gor'kov equation in this appendix.

A.1 Matsubara Green's Functions

The Matsubara Green's function is defined for imaginary time $t = i\tau$ within the interval $-1/T < \tau_1 - \tau_2 < 1/T$.

Heisenberg particle operators depending on time τ are defined as:

$$\tilde{\psi}_\alpha(\mathbf{r}, \tau) = e^{(\hat{H} - \mu\hat{N})\tau} \psi_\alpha(\mathbf{r}) e^{-(\hat{H} - \mu\hat{N})\tau}, \quad (\text{A.1a})$$

$$\tilde{\psi}_\alpha^\dagger(\mathbf{r}, \tau) = e^{(\hat{H} - \mu\hat{N})\tau} \psi_\alpha^\dagger(\mathbf{r}) e^{-(\hat{H} - \mu\hat{N})\tau}. \quad (\text{A.1b})$$

These operators obey the normal Fermionic relations,

$$\left\{ \tilde{\psi}_\alpha(\mathbf{r}_1, \tau), \tilde{\psi}_\beta^\dagger(\mathbf{r}_2, \tau) \right\} = \delta_{\alpha\beta} \delta(\mathbf{r}_1 - \mathbf{r}_2), \quad (\text{A.2a})$$

$$\left\{ \tilde{\psi}_\alpha(\mathbf{r}_1, \tau), \tilde{\psi}_\beta(\mathbf{r}_2, \tau) \right\} = \left\{ \tilde{\psi}_\alpha^\dagger(\mathbf{r}_1, \tau), \tilde{\psi}_\beta^\dagger(\mathbf{r}_2, \tau) \right\} = 0, \quad (\text{A.2b})$$

where, commutation of operator A and B is defined as $[A, B] = AB - BA$ and anticommutation is defined as $\{A, B\} = AB + BA$.

The equations of motion of the Heisenberg particle operators are:

$$\frac{\partial \tilde{\psi}_\alpha}{\partial \tau} = [\hat{H} - \mu \hat{N}, \tilde{\psi}_\alpha], \quad (\text{A.3a})$$

$$\frac{\partial \tilde{\psi}_\alpha^\dagger}{\partial \tau} = [\hat{H} - \mu \hat{N}, \tilde{\psi}_\alpha^\dagger]. \quad (\text{A.3b})$$

With above definitions, we can define a single particle Green's function as:

$$\begin{aligned} G_{\alpha\beta}(\mathbf{r}_1, \tau_1; \mathbf{r}_2, \tau_2) &\equiv \left\langle T_\tau \left(\tilde{\psi}_\alpha(\mathbf{r}_1, \tau_1) \tilde{\psi}_\beta^\dagger(\mathbf{r}_2, \tau_2) \right) \right\rangle, \\ &= -\langle \tilde{\psi}_\alpha(\mathbf{r}_1, \tau_1) \tilde{\psi}_\beta^\dagger(\mathbf{r}_2, \tau_2) \rangle \Theta(\tau_1 - \tau_2) + \langle \tilde{\psi}_\beta^\dagger(\mathbf{r}_2, \tau_2) \tilde{\psi}_\alpha(\mathbf{r}_1, \tau_1) \rangle \Theta(\tau_2 - \tau_1). \end{aligned} \quad (\text{A.4})$$

Where, T_τ means ordering operators $\tilde{\psi}(\tau)$ from left to right in order of decreasing τ . For example, $T_\tau \left(\tilde{\psi}_1 \tilde{\psi}_2^\dagger \right) = \begin{cases} \tilde{\psi}_1 \tilde{\psi}_2^\dagger & \text{for } \tau_1 > \tau_2, \\ -\tilde{\psi}_2^\dagger \tilde{\psi}_1 & \text{for } \tau_1 < \tau_2. \end{cases}$. The operator $\langle \dots \rangle$ is the

Gibbs statistical average, defined as $\langle \dots \rangle \equiv \sum \left[\exp\left(\frac{\Omega + \mu \hat{N} - \hat{H}}{T}\right) \dots \right]$. $\Omega = F - \mu N$ and $F = -T \ln \sum_n e^{-E_n/T}$.

Important features of G with time difference $\tau = \tau_1 - \tau_2$ include:

$$G_{\alpha\beta}(\mathbf{r}_1, \tau_1; \mathbf{r}_2, \tau_2) = G_{\alpha\beta}(\mathbf{r}_1, \mathbf{r}_2; \tau), \quad (\text{A.5})$$

$$G_{\alpha\beta}(\mathbf{r}_1, \mathbf{r}_2; \tau < 0) = -G_{\alpha\beta}(\mathbf{r}_1, \mathbf{r}_2; \tau + 1/T), \quad (\text{A.6})$$

$$(G_{\alpha\beta}(\mathbf{r}_1, \mathbf{r}_2; \tau) - G_{\alpha\beta}(\mathbf{r}_1, \mathbf{r}_2; -\tau))_{\tau \rightarrow 0^+} = \delta_{\alpha\beta} \delta(\mathbf{r}_1 - \mathbf{r}_2). \quad (\text{A.7})$$

The Fourier transformation of G in τ or ω_n goes to:

$$G_{\alpha\beta}(\mathbf{r}_1, \mathbf{r}_2; \tau) = T \sum_{n=-\infty}^{\infty} e^{i\omega_n \tau} G_{\alpha\beta}(\mathbf{r}_1, \mathbf{r}_2; \omega_n); \quad (\text{A.8})$$

$$G_{\alpha\beta}(\mathbf{r}_1, \mathbf{r}_2; \omega_n) = \frac{1}{2} \int_{-1/T}^{1/T} d\tau e^{i\omega_n \tau} G_{\alpha\beta}(\mathbf{r}_1, \mathbf{r}_2; \tau). \quad (\text{A.9})$$

As τ is defined within a finite range, the ω_n should be discrete: $\omega_n = n\pi T$. The discrete frequencies are called Matsubara frequencies.

With relation Eq.(A.6), we can get:

$$\begin{aligned} G_{\alpha\beta}(\mathbf{r}_1, \mathbf{r}_2; \omega_n) &= \frac{1}{2} \int_0^{1/T} d\tau e^{i\omega_n \tau} G_{\alpha\beta}(\mathbf{r}_1, \mathbf{r}_2; \tau) + \frac{1}{2} \int_{-1/T}^0 d\tau e^{i\omega_n \tau} G_{\alpha\beta}(\mathbf{r}_1, \mathbf{r}_2; \tau) \\ &= \int_0^{1/T} d\tau e^{i\omega_n \tau} G_{\alpha\beta}(\mathbf{r}_1, \mathbf{r}_2; \tau), \end{aligned} \quad (\text{A.10})$$

with Matsubara frequencies $\omega_n = (2n + 1)\pi T$ for Fermions.

A.2 Gor'kov Equation

The BCS Hamiltonian is:

$$\hat{H}_{BCS} = \int d^3r \left[-\psi_\alpha^\dagger \frac{\nabla^2}{2m} \psi_\alpha + \frac{g}{2} \psi_\beta^\dagger \psi_\alpha^\dagger \psi_\alpha \psi_\beta \right]. \quad (\text{A.11})$$

The equation of motion of operators $\tilde{\psi}$ are:

$$\frac{\partial \tilde{\psi}_\alpha(\mathbf{r}, \tau)}{\partial \tau} = \left(\frac{\nabla^2}{2m} + \mu \right) \tilde{\psi}_\alpha(\mathbf{r}, \tau) - g \tilde{\psi}_\gamma^\dagger(\mathbf{r}, \tau) \tilde{\psi}_\gamma(\mathbf{r}, \tau) \tilde{\psi}_\alpha(\mathbf{r}, \tau), \quad (\text{A.12a})$$

$$\frac{\partial \tilde{\psi}_\alpha^\dagger(\mathbf{r}, \tau)}{\partial \tau} = \left(\frac{\nabla^2}{2m} + \mu \right) \tilde{\psi}_\alpha^\dagger(\mathbf{r}, \tau) - g \tilde{\psi}_\alpha^\dagger(\mathbf{r}, \tau) \tilde{\psi}_\gamma^\dagger(\mathbf{r}, \tau) \tilde{\psi}_\gamma(\mathbf{r}, \tau). \quad (\text{A.12b})$$

With the particle number operator defined as: $\hat{N} = \int d^3r \psi_\alpha^\dagger \psi_\alpha$.

The time-derivative of G can be expressed as:

$$\begin{aligned} \frac{\partial G_{\alpha\beta}(\mathbf{r}_1, \tau_1; \mathbf{r}_2, \tau_2)}{\partial \tau_1} &= -\delta(\tau_1 - \tau_2) \left(\left\langle \tilde{\psi}_\alpha(\mathbf{r}_1, \tau_1) \tilde{\psi}_\beta^\dagger(\mathbf{r}_2, \tau_2) + \tilde{\psi}_\beta^\dagger(\mathbf{r}_2, \tau_2) \tilde{\psi}_\alpha(\mathbf{r}_1, \tau_1) \right\rangle \right) \\ &\quad - \left\langle T_\tau \frac{\partial \tilde{\psi}_\alpha(\mathbf{r}_1, \tau_1)}{\partial \tau_1} \tilde{\psi}_\beta^\dagger(\mathbf{r}_2, \tau_2) \right\rangle \\ &= \delta_{\alpha\beta} \delta(\mathbf{r}_1 - \mathbf{r}_2) \delta(\tau_1 - \tau_2) + \left(\frac{\nabla^2}{2m} + \mu \right) G_{\alpha\beta}(\mathbf{r}_1, \tau_1; \mathbf{r}_2, \tau_2) \\ &\quad - g \left\langle T_\tau \tilde{\psi}_\gamma^\dagger(\mathbf{r}_1, \tau_1) \tilde{\psi}_\gamma(\mathbf{r}_1, \tau_1) \tilde{\psi}_\alpha(\mathbf{r}_1, \tau_1) \tilde{\psi}_\beta^\dagger(\mathbf{r}_2, \tau_2) \right\rangle. \end{aligned} \quad (\text{A.13})$$

We can apply the Wick theorem¹ to decompose the four-operator average $\langle \tilde{\psi}^\dagger \tilde{\psi} \tilde{\psi} \tilde{\psi}^\dagger \rangle$

1

$$\begin{aligned} \left\langle T_\tau \tilde{\psi}_\gamma^\dagger(\mathbf{r}_1, \tau_1) \tilde{\psi}_\gamma(\mathbf{r}_1, \tau_1) \tilde{\psi}_\alpha(\mathbf{r}_1, \tau_1) \tilde{\psi}_\beta^\dagger(\mathbf{r}_2, \tau_2) \right\rangle &= - \left\langle \tilde{\psi}_\gamma(\mathbf{r}_1, \tau_1) \tilde{\psi}_\gamma^\dagger(\mathbf{r}_1, \tau_1) \right\rangle \left\langle T_\tau \tilde{\psi}_\alpha(\mathbf{r}_1, \tau_1) \tilde{\psi}_\beta^\dagger(\mathbf{r}_2, \tau_2) \right\rangle \\ &\quad + \left\langle \tilde{\psi}_\alpha(\mathbf{r}_1, \tau_1) \tilde{\psi}_\gamma^\dagger(\mathbf{r}_1, \tau_1) \right\rangle \left\langle T_\tau \tilde{\psi}_\gamma(\mathbf{r}_1, \tau_1) \tilde{\psi}_\beta^\dagger(\mathbf{r}_2, \tau_2) \right\rangle \\ &\quad - \left\langle \tilde{\psi}_\alpha(\mathbf{r}_1, \tau_1) \tilde{\psi}_\gamma(\mathbf{r}_1, \tau_1) \right\rangle \left\langle T_\tau \tilde{\psi}_\gamma^\dagger(\mathbf{r}_1, \tau_1) \tilde{\psi}_\beta^\dagger(\mathbf{r}_2, \tau_2) \right\rangle \end{aligned}$$

in Eq.A.13 in terms of products of operator pairs $\langle \tilde{\psi}^\dagger \tilde{\psi}^\dagger \rangle$, $\langle \tilde{\psi} \tilde{\psi} \rangle$ and $\langle \tilde{\psi} \tilde{\psi}^\dagger \rangle$. The terms only associated with $\tilde{\psi} \tilde{\psi}^\dagger$ can be neglected, as they won't contribute to the superconductivity. Finally, we get:

$$\begin{aligned} \left(\frac{\partial}{\partial \tau_1} - \frac{\nabla^2}{2m} - \mu \right) G_{\alpha\beta}(\mathbf{r}_1, \tau_1; \mathbf{r}_2, \tau_2) - g \left\langle \tilde{\psi}_\alpha(\mathbf{r}_1, \tau_1) \tilde{\psi}_\gamma(\mathbf{r}_1, \tau_1) \right\rangle \left\langle T_\tau \tilde{\psi}_\gamma^\dagger(\mathbf{r}_1, \tau_1) \tilde{\psi}_\beta^\dagger(\mathbf{r}_2, \tau_2) \right\rangle \\ = \delta_{\alpha\beta} \delta(\mathbf{r}_1 - \mathbf{r}_2) \delta(\tau_1 - \tau_2). \end{aligned} \quad (\text{A.14})$$

Anomalous Green's functions can be introduced here and defined as:

$$F_{\alpha\beta}(\mathbf{r}_1, \tau_1; \mathbf{r}_2, \tau_2) = \left\langle T_\tau \left(\tilde{\psi}_\alpha(\mathbf{r}_1, \tau_1) \tilde{\psi}_\beta(\mathbf{r}_2, \tau_2) \right) \right\rangle, \quad (\text{A.15a})$$

$$F_{\alpha\beta}^\dagger(\mathbf{r}_1, \tau_1; \mathbf{r}_2, \tau_2) = \left\langle T_\tau \left(\tilde{\psi}_\alpha^\dagger(\mathbf{r}_1, \tau_1) \tilde{\psi}_\beta^\dagger(\mathbf{r}_2, \tau_2) \right) \right\rangle. \quad (\text{A.15b})$$

The superconducting order parameter can be expressed in terms of the anomalous Green's functions F and F^\dagger as,

$$\Delta_{\alpha\beta}(\mathbf{r}) = |g| F_{\alpha\beta}(\mathbf{r}, \tau; \mathbf{r}, \tau), \quad (\text{A.16a})$$

$$\Delta_{\alpha\beta}^\dagger(\mathbf{r}) = |g| F_{\alpha\beta}^\dagger(\mathbf{r}, \tau; \mathbf{r}, \tau), \quad (\text{A.16b})$$

where $g < 0$ represent attractive interaction.

The equation for the Green's functions, Eq.(A.14), can be rewritten as:

$$\begin{aligned} \left(\frac{\partial}{\partial \tau_1} - \frac{\nabla^2}{2m} - \mu \right) G_{\alpha\beta}(\mathbf{r}_1, \tau_1; \mathbf{r}_2, \tau_2) + \Delta_{\alpha\gamma}(\mathbf{r}_1, \tau_1) F_{\gamma\beta}^\dagger(\mathbf{r}_1, \tau_1; \mathbf{r}_2, \tau_2) \\ = \delta_{\alpha\beta} \delta(\mathbf{r}_1 - \mathbf{r}_2) \delta(\tau_1 - \tau_2). \end{aligned} \quad (\text{A.17})$$

Switching the spin labels in G , Δ and F , we can get:

$$G_{\alpha\beta}(\mathbf{r}_1, \tau_1; \mathbf{r}_2, \tau_2) = \delta_{\alpha\beta} G(\mathbf{r}_1, \tau_1; \mathbf{r}_2, \tau_2); \quad (\text{A.18})$$

$$\Delta_{\alpha\beta}(\mathbf{r}, \tau) = \begin{cases} -\Delta_{\beta\alpha}(\mathbf{r}, \tau) = i\hat{\sigma}_{\alpha\beta}^{(2)}\Delta(\mathbf{r}, \tau) & \text{for a spin-singlet,} \\ \Delta_{\beta\alpha}(\mathbf{r}, \tau) = \hat{\sigma}_{\alpha\beta}^{(1)}\Delta(\mathbf{r}, \tau) & \text{for a spin-triplet;} \end{cases} \quad (\text{A.19})$$

$$F_{\alpha\beta}(\mathbf{r}_1, \tau_1; \mathbf{r}_2, \tau_2) = \begin{cases} i\hat{\sigma}_{\alpha\beta}^{(2)}F(\mathbf{r}_1, \tau_1; \mathbf{r}_2, \tau_2) & \text{for a spin-singlet,} \\ \hat{\sigma}_{\alpha\beta}^{(1)}F(\mathbf{r}_1, \tau_1; \mathbf{r}_2, \tau_2) & \text{for a spin-triplet;} \end{cases} \quad (\text{A.20})$$

where, $\hat{\sigma}_{\alpha\beta}^{(1)}$ and $\hat{\sigma}_{\alpha\beta}^{(2)}$ are Pauli matrices,

$$\hat{\sigma}_{\alpha\beta}^{(1)} = \begin{pmatrix} 0 & 1 \\ 1 & 0 \end{pmatrix}, \quad \hat{\sigma}_{\alpha\beta}^{(2)} = \begin{pmatrix} 0 & -i \\ i & 0 \end{pmatrix}. \quad (\text{A.21})$$

Eq.(A.17) can be simplified to the spinless case from for both spin-singlet and spin-triplet cases:

$$\left(\frac{\partial}{\partial\tau_1} - \frac{\nabla^2}{2m} - \mu \right) G(\mathbf{r}_1, \tau_1; \mathbf{r}_2, \tau_2) + \Delta(\mathbf{r}_1, \tau_1)F^\dagger(\mathbf{r}_1, \tau_1; \mathbf{r}_2, \tau_2) = \delta(\mathbf{r}_1 - \mathbf{r}_2)\delta(\tau_1 - \tau_2). \quad (\text{A.22})$$

Note that equations for F and F^\dagger are required to calculate G and these equations

can be obtained using the same process,

$$\left(-\frac{\partial}{\partial\tau_1} + \frac{\nabla^2}{2m} + \mu\right)F(\mathbf{r}_1, \tau_1; \mathbf{r}_2, \tau_2) + \Delta(\mathbf{r}_1, \tau_1)\bar{G}(\mathbf{r}_1, \tau_1; \mathbf{r}_2, \tau_2) = 0, \quad (\text{A.23})$$

$$\left(\frac{\partial}{\partial\tau_1} + \frac{\nabla^2}{2m} + \mu\right)F^\dagger(\mathbf{r}_1, \tau_1; \mathbf{r}_2, \tau_2) + \Delta^*(\mathbf{r}_1, \tau_1)G(\mathbf{r}_1, \tau_1; \mathbf{r}_2, \tau_2) = 0, \quad (\text{A.24})$$

$$-\left(\frac{\partial}{\partial\tau_1} + \frac{\nabla^2}{2m} + \mu\right)\bar{G}(\mathbf{r}_1, \tau_1; \mathbf{r}_2, \tau_2) + \Delta^*(\mathbf{r}_1, \tau_1)F(\mathbf{r}_1, \tau_1; \mathbf{r}_2, \tau_2) = \delta(\mathbf{r}_1 - \mathbf{r}_2)\delta(\tau_1 - \tau_2). \quad (\text{A.25})$$

Where, $\bar{G}(\mathbf{r}_1, \tau_1; \mathbf{r}_2, \tau_2) = G(\mathbf{r}_2, \tau_2; \mathbf{r}_1, \tau_1)$ describes a hole moving from \mathbf{r}_2 to \mathbf{r}_1 . Eq.(A.22)-A.25 are known as the Gor'kov equations.

We can introduce the matrix Green's function,

$$\hat{G}(\mathbf{r}_1, \tau_1; \mathbf{r}_2, \tau_2) = \begin{pmatrix} G(\mathbf{r}_1, \tau_1; \mathbf{r}_2, \tau_2) & F(\mathbf{r}_1, \tau_1; \mathbf{r}_2, \tau_2) \\ -F^\dagger(\mathbf{r}_1, \tau_1; \mathbf{r}_2, \tau_2) & \bar{G}(\mathbf{r}_1, \tau_1; \mathbf{r}_2, \tau_2) \end{pmatrix}, \quad (\text{A.26})$$

and rewrite the Gor'kov equations, in the matrix form, as:

$$\begin{pmatrix} \frac{\partial}{\partial\tau_1} - \frac{\nabla^2}{2m} - \mu & -\Delta(\mathbf{r}_1, \tau_1) \\ \Delta^*(\mathbf{r}_1, \tau_1) & -\frac{\partial}{\partial\tau_1} - \frac{\nabla^2}{2m} - \mu \end{pmatrix} \hat{G}(\mathbf{r}_1, \tau_1; \mathbf{r}_2, \tau_2) = \delta(\mathbf{r}_1 - \mathbf{r}_2)\delta(\tau_1 - \tau_2)\hat{1}, \quad (\text{A.27})$$

where $\hat{1} = \begin{pmatrix} 1 & 0 \\ 0 & 1 \end{pmatrix}$.

Repeating the whole procedure for τ_2 , we get:

$$\hat{G}(\mathbf{r}_1, \tau_1; \mathbf{r}_2, \tau_2) \begin{pmatrix} -\frac{\partial}{\partial\tau_2} - \frac{\nabla^2}{2m} - \mu & -\Delta(\mathbf{r}_2, \tau_2) \\ \Delta^*(\mathbf{r}_2, \tau_2) & \frac{\partial}{\partial\tau_2} - \frac{\nabla^2}{2m} - \mu \end{pmatrix} = \delta(\mathbf{r}_1 - \mathbf{r}_2)\delta(\tau_1 - \tau_2)\hat{1}. \quad (\text{A.28})$$

In the presence of a magnetic field, the Gor'kov equation can be rewritten as,

$$\begin{pmatrix} \frac{\partial}{\partial \tau_1} + H & -\Delta(\mathbf{r}_1, \tau_1) \\ \Delta^*(\mathbf{r}_1, \tau_1) & -\frac{\partial}{\partial \tau_1} + H^* \end{pmatrix} \hat{G}(\mathbf{r}_1, \tau_1; \mathbf{r}_2, \tau_2) = \delta(\mathbf{r}_1 - \mathbf{r}_2) \delta(\tau_1 - \tau_2) \hat{1}, \quad (\text{A.29a})$$

$$\hat{G}(\mathbf{r}_1, \tau_1; \mathbf{r}_2, \tau_2) \begin{pmatrix} -\frac{\partial}{\partial \tau_2} + H^* & -\Delta(\mathbf{r}_2, \tau_2) \\ \Delta^*(\mathbf{r}_2, \tau_2) & \frac{\partial}{\partial \tau_2} + H \end{pmatrix} = \delta(\mathbf{r}_1 - \mathbf{r}_2) \delta(\tau_1 - \tau_2) \hat{1}, \quad (\text{A.29b})$$

where, $H = (-i\nabla + \frac{e}{c}\mathbf{A})^2 / 2m - \mu$.

Applying the Fourier Transform (Eq.(A.9)), we get the Gor'kov equation in the frequency representation,

$$\begin{pmatrix} -i\omega_n + H & -\Delta(\mathbf{r}_1) \\ \Delta^*(\mathbf{r}_1) & i\omega_n + H^* \end{pmatrix} \hat{G}(\mathbf{r}_1, \mathbf{r}_2; \omega_n) = \delta(\mathbf{r}_1 - \mathbf{r}_2) \hat{1}, \quad (\text{A.30a})$$

$$\hat{G}(\mathbf{r}_1, \mathbf{r}_2; \omega_n) \begin{pmatrix} -i\omega_n + H^* & -\Delta(\mathbf{r}_2) \\ \Delta^*(\mathbf{r}_2) & +i\omega_n + H \end{pmatrix} = \delta(\mathbf{r}_1 - \mathbf{r}_2) \hat{1}. \quad (\text{A.30b})$$

Bibliography

- [1] J. Bardeen, L. N. Cooper, and J. R. Schrieffer, “Theory of superconductivity,” *Phys. Rev.*, vol. 108, pp. 1175–1204, Dec 1957.
- [2] L. D. Landau and V. L. Ginzburg, “On the theory of superconductivity,” *Zh. Eksp. Teor. Fiz.*, vol. 20, p. 1064, 1950.
- [3] J. G. Bednorz and K. A. Müller, “Possible high T_c superconductivity in the Ba-La-Cu-O system,” *Zeitschrift für Physik B Condensed Matter*, vol. 64, pp. 189–193, Jun 1986.
- [4] C. Kallin, “Chiral p -wave order in Sr_2RuO_4 ,” *Reports on Progress in Physics*, vol. 75, no. 4, p. 042501, 2012.
- [5] C. Kallin and J. Berlinsky, “Chiral superconductors,” *Reports on Progress in Physics*, vol. 79, no. 5, p. 054502, 2016.
- [6] M. Z. Hasan and C. L. Kane, “Colloquium: Topological insulators,” *Rev. Mod. Phys.*, vol. 82, pp. 3045–3067, Nov 2010.
- [7] X. L. Qi and S. C. Zhang, “Topological insulators and superconductors,” *Rev. Mod. Phys.*, vol. 83, pp. 1057–1110, Oct 2011.

- [8] M. Stone and R. Roy, “Edge modes, edge currents, and gauge invariance in p_x+ip_y superfluids and superconductors,” *Phys. Rev. B*, vol. 69, p. 184511, May 2004.
- [9] N. Read and D. Green, “Paired states of fermions in two dimensions with breaking of parity and time-reversal symmetries and the fractional quantum hall effect,” *Phys. Rev. B*, vol. 61, pp. 10267–10297, Apr 2000.
- [10] C. Nayak, S. H. Simon, A. Stern, M. Freedman, and S. D. Sarma, “Non-abelian anyons and topological quantum computation,” *Rev. Mod. Phys.*, vol. 80, pp. 1083–1159, Sep 2008.
- [11] D. A. Ivanov, “Non-abelian statistics of half-quantum vortices in p -wave superconductors,” *Phys. Rev. Lett.*, vol. 86, pp. 268–271, Jan 2001.
- [12] G. M. Luke, Y. Fudamoto, K. M. Kojima, M. I. Larkin, J. Merrin, B. Nachumi, Y. J. Uemura, Y. Maeno, Z. Q. Mao, Y. Mori, H. Nakamura, and M. Sigrist, “Time-reversal symmetry-breaking superconductivity in Sr_2RuO_4 ,” *Nature*, vol. 394, pp. 558–561, Aug 1998.
- [13] J. Xia, Y. Maeno, P. T. Beyersdorf, M. M. Fejer, and A. Kapitulnik, “High resolution polar kerr effect measurements of Sr_2RuO_4 : Evidence for broken time-reversal symmetry in the superconducting state,” *Phys. Rev. Lett.*, vol. 97, p. 167002, Oct 2006.
- [14] R. Jackiw and C. Rebbi, “Solitons with fermion number $1/2$,” *Phys. Rev. D*, vol. 13, pp. 3398–3409, Jun 1976.

- [15] T. Kita, “Angular momentum of anisotropic superfluids at finite temperatures,” *Journal of the Physical Society of Japan*, vol. 67, no. 1, pp. 216–224, 1998.
- [16] J. A. Sauls, “Surface states, edge currents, and the angular momentum of chiral p -wave superfluids,” *Phys. Rev. B*, vol. 84, p. 214509, Dec 2011.
- [17] W. Huang, E. Taylor, and C. Kallin, “Vanishing edge currents in non- p -wave topological chiral superconductors,” *Phys. Rev. B*, vol. 90, p. 224519, Dec 2014.
- [18] Y. Tada, W. Nie, and M. Oshikawa, “Orbital angular momentum and spectral flow in two-dimensional chiral superfluids,” *Phys. Rev. Lett.*, vol. 114, p. 195301, May 2015.
- [19] W. Huang, S. Lederer, E. Taylor, and C. Kallin, “Nontopological nature of the edge current in a chiral p -wave superconductor,” *Phys. Rev. B*, vol. 91, p. 094507, Mar 2015.
- [20] A. J. Leggett, *Quantum liquids: Bose condensation and Cooper pairing in condensed-matter systems*. Oxford University Press, 2006.
- [21] D. Rainer, H. Burkhardt, M. Fogelström, and J. Sauls, “Andreev bound states, surfaces and subdominant pairing in high T_c superconductors,” *Journal of Physics and Chemistry of Solids*, vol. 59, no. 10, pp. 2040 – 2044, 1998.
- [22] B. Braunecker, P. A. Lee, and Z. Wang, “Edge currents in superconductors with a broken time-reversal symmetry,” *Phys. Rev. Lett.*, vol. 95, p. 017004, Jul 2005.
- [23] M. Matsumoto and M. Sigrist, “Quasiparticle states near the surface and the domain wall in a $p_x \pm ip_y$ -wave superconductor,” *Journal of the Physical Society of Japan*, vol. 68, no. 3, pp. 994–1007, 1999.

- [24] S. Suzuki and Y. Asano, “Spontaneous edge current in a small chiral superconductor with a rough surface,” *Phys. Rev. B*, vol. 94, p. 155302, Oct 2016.
- [25] J. R. Kirtley, C. Kallin, C. W. Hicks, E.-A. Kim, Y. Liu, K. A. Moler, Y. Maeno, and K. D. Nelson, “Upper limit on spontaneous supercurrents in Sr_2RuO_4 ,” *Phys. Rev. B*, vol. 76, p. 014526, Jul 2007.
- [26] C. W. Hicks, J. R. Kirtley, T. M. Lippman, N. C. Koshnick, M. E. Huber, Y. Maeno, W. M. Yuhasz, M. B. Maple, and K. A. Moler, “Limits on superconductivity-related magnetization in Sr_2RuO_4 and $\text{PrOs}_4\text{Sb}_{12}$ from scanning SQUID microscopy,” *Phys. Rev. B*, vol. 81, p. 214501, Jun 2010.
- [27] S. J. Ray, A. S. Gibbs, S. J. Bending, P. J. Curran, E. Babaev, C. Baines, A. P. Mackenzie, and S. L. Lee, “Muon-spin rotation measurements of the vortex state in Sr_2RuO_4 : Type-1.5 superconductivity, vortex clustering, and a crossover from a triangular to a square vortex lattice,” *Phys. Rev. B*, vol. 89, p. 094504, Mar 2014.
- [28] Y. Nagato, M. Yamamoto, and K. Nagai, “Rough surface effects on the p -wave fermi superfluids,” *Journal of low temperature physics*, vol. 110, pp. 1135–1171, Mar 1998.
- [29] P. E. C. Ashby and C. Kallin, “Suppression of spontaneous supercurrents in a chiral p -wave superconductor,” *Phys. Rev. B*, vol. 79, p. 224509, Jun 2009.
- [30] Y. Nagato, S. Higashitani, and K. Nagai, “Subgap in the edge states of two-dimensional chiral superconductor with rough surface,” *Journal of the Physical Society of Japan*, vol. 80, no. 11, p. 113706, 2011.

- [31] S. V. Bakurskiy, A. A. Golubov, M. Y. Kupriyanov, K. Yada, and Y. Tanaka, “Anomalous surface states at interfaces in p -wave superconductors,” *Phys. Rev. B*, vol. 90, p. 064513, Aug 2014.
- [32] S. Lederer, W. Huang, E. Taylor, S. Raghu, and C. Kallin, “Suppression of spontaneous currents in Sr_2RuO_4 by surface disorder,” *Phys. Rev. B*, vol. 90, p. 134521, Oct 2014.
- [33] S. V. Bakurskiy, N. V. Klenov, I. I. Soloviev, K. M. Yu., and A. A. Golubov, “Observability of surface currents in p -wave superconductors,” *Superconductor Science and Technology*, vol. 30, no. 4, p. 044005, 2017.
- [34] L. P. Gorkov, “Microscopic derivation of the Ginzburg-Landau equations in the theory of superconductivity,” *Sov. Phys. JETP*, vol. 9, no. 6, pp. 1364–1367, 1959.
- [35] G. Eilenberger, “Transformation of Gorkov’s equation for type II superconductors into transport-like equations,” *Zeitschrift für Physik A Hadrons and nuclei*, vol. 214, pp. 195–213, Apr 1968.
- [36] A. I. Larkin and Y. N. Ovchinnikov, “Quasiclassical method in the theory of superconductivity,” *Sov Phys JETP*, vol. 28, no. 6, pp. 1200–1205, 1969.
- [37] A. Zaitsev, “Quasiclassical equations of the theory of superconductivity for contiguous metals and the properties of constricted microcontacts,” *Zh. Eksp. Teor. Fiz*, vol. 86, pp. 1742–1758, 1984.
- [38] N. Schopohl and K. Maki, “Quasiparticle spectrum around a vortex line in a d -wave superconductor,” *Phys. Rev. B*, vol. 52, pp. 490–493, Jul 1995.

- [39] M. Ichioka, N. Hayashi, N. Enomoto, and K. Machida, “Vortex structure in d -wave superconductors,” *Phys. Rev. B*, vol. 53, pp. 15316–15326, Jun 1996.
- [40] M. Ichioka, A. Hasegawa, and K. Machida, “Vortex lattice effects on low-energy excitations in d -wave and s -wave superconductors,” *Phys. Rev. B*, vol. 59, pp. 184–187, Jan 1999.
- [41] M. Ichioka and K. Machida, “Field dependence of the vortex structure in chiral p -wave superconductors,” *Phys. Rev. B*, vol. 65, p. 224517, Jun 2002.
- [42] A. A. Abrikosov, L. P. Gorkov, and I. E. Dzyaloshinski, *Methods of quantum field theory in statistical physics*. Courier Corporation, 2012.
- [43] N. B. Kopnin, *Theory of nonequilibrium superconductivity*, vol. 110. Oxford University Press, 2001.
- [44] T. Kita, *Statistical mechanics of superconductivity*. Springer, 2015.
- [45] N. Schopohl, “Transformation of the Eilenberger equations of superconductivity to a scalar Riccati equation,” *arXiv preprint cond-mat/9804064*, 1998.
- [46] M. Matsumoto and H. Shiba, “Coexistence of different symmetry order parameters near a surface in d -wave superconductors I,” *Journal of the Physical Society of Japan*, vol. 64, no. 9, pp. 3384–3396, 1995.
- [47] M. Matsumoto and H. Shiba, “Coexistence of different symmetry order parameters near a surface in d -wave superconductors II,” *Journal of the Physical Society of Japan*, vol. 64, no. 12, pp. 4867–4881, 1995.

- [48] M. Matsumoto and H. Shiba, “Coexistence of different symmetry order parameters near a surface in d -wave superconductors III,” *Journal of the Physical Society of Japan*, vol. 65, no. 7, pp. 2194–2203, 1996.
- [49] W. Huang, *Theoretical studies of unconventional superconductivity in Sr_2RuO_4* . PhD thesis, McMaster University, 2016.
- [50] L. S. Borkowski and P. J. Hirschfeld, “Distinguishing d -wave superconductors from highly anisotropic s -wave superconductors,” *Phys. Rev. B*, vol. 49, pp. 15404–15407, Jun 1994.